THE STRESS DISTRIBUTION AT THE BOUNDARY OF AN OVALOID HOLE IN WEBS SUBJECTED TO COMBINED BENDING AND SHEAR

RICHARD PENDLETON HALL
ROLAND FIELD WILKINSON

THE STRESS DISTRIBUTION AT THE BOUNDARY OF AN OVALOID HOLE IN WEBS SUBJECTED TO COMBINED BENDING AND SHEAR

By

Richard Pendleton Hall
Lieutenant (j.g.), U.S.Navy
B.S., U.S.Naval Academy, 1945

Roland Field Wilkinson
Lieutenant (j.g.), U.S.Navy

Submitted in Partial Fulfillment of
the Requirements for the Degree of

NAVAL ENGINEER

from the
MASSACHUSETTS INSTITUTE OF TECHNOLOGY
(1951)

ABSTRACT

A. Title: The Stress Distribution at the Boundary of an Ovaloid Hole in Web Subjected to Combined Bending and Shear.

B. Authors: Roland Field Wilkinson
Richard Pendleton Hall

C. Submitted for the Degree of Naval Engineer in the Department of Naval Architecture and Marine Engineering on 18 May 1951.

D. The object of this thesis is to determine, by photoelastic methods, the stress distribution at the boundary of an ovaloid hole in webs of different depths, subjected to various ratios of shear to bending stress. The results, in the form of plots, were compared with the Heller and secondary bending formulae. A simple formula for determining the maximum stress at the ovaloid boundary was also devised.

The plots show that good agreement exists between Heller's predicted stress and the observed values for all ratios of shear to bending stress, and for hole-web depth ratios less than about 0.25. At hole-web depth ratios greater than 0.30, it is indicated that the stress predicted by the secondary bending theory exceeds the observed values.

Cambridge, Massachusetts

May 18, 1951

Professor J. S. Newell
Secretary of the Faculty
Massachusetts Institute of Technology
Cambridge, Massachusetts

Dear Sir:

In accordance with the requirements for the degree of Naval Engineer we submit herewith a thesis entitled "The Stress Distribution at the Boundary of an Ovaloid Hole in Webs Subjected to Combined Bending and Shear."

Respectfully submitted,

TABLE OF CONTENTS

SUMMARY

The object of this thesis is threefold:

1. To determine experimentally the stress distribution at the boundary of an ovaloid hole in webs of different depths subjected to various ratios of shear to bending stress.
2. To determine how closely the stress distribution for the above conditions predicted by the Heller and secondary bending formulae (see Appendix "A") agree with the observed distribution.
3. To devise a simple expression for the determination of the maximum stress at the ovaloid boundary for use in structural design.

The experimental results were obtained by photoelastic analysis. Figures II-XXVIII indicate the observed stress distribution at the boundary of an ovaloid of aspect ratio 2.0 in webs of different depths subjected to various ratios of shear to bending stress. These figures further evince that good agreement exists between Heller's predicted stress and the observed values for all ratios of shear to bending stress and hole-web depth ratios less than about .25. At hole-web depth ratios greater than about .30 it is indicated that the stress predicted by the secondary bending theory exceeds the observed values.

Figures XXIX-XXXIII depict the maximum observed and predicted values of stress at the hole boundary for various ratios of hole-web depth and shear-bending stress ratios. It may be assumed that conservative structural design will result by the use of the secondary bending theory for hole-web depth ratios greater than about .30 and Heller's equation for ratios less than about .25.

The following formulae (see Nomenclature, Appendix "C") are suggested for rapid determination of the maximum stress at the ovaloid boundary:

When the hole-web depth ratio is less than about .25 and the value of the shear-bending stress ratio <u>greater</u> than about .10:

$$\left(\frac{\sigma_t}{\sigma_o}\right)_{MAX.} \cong 10.0\left(\frac{c}{b}\right)^{0.8}\frac{\tau}{\sigma}$$

When the hole-web depth ratio is less than about .25 and the value of the shear-bending stress ratio <u>less</u> than about .10:

$$\left(\frac{\sigma_t}{\sigma_c}\right)_{MAX.} \cong 1.30^{*} + e^{4.3\left(\frac{c}{b}\right)^{0.65}}\frac{\tau}{\sigma}$$

When the hole-web depth ratio is greater than about .30 and the shear-bending stress ratio <u>greater</u> than about .10 a value of $\ell = b - \frac{r}{2}$ should be substituted in the secondary bending stress formula. When the shear-bending stress ra-

*The experimental and theoretical results of Heller (Ref.No.6) indicate that the max.stress concentration for pure bending($\tau/\sigma = 0$ should be about 1.30;hence this value is used in light of the random variation of the extrapolated values at $\tau/\sigma = 0$ in Figs. XXIX-XXXIII.

tio is less than about .10 it is known only that "ℓ" increases with the shear-bending stress ratio between values of something more than zero and less than $b-\frac{r}{2}$.

Summarizing, it is concluded that:

1. Heller's solution for the stress at the boundary of an ovaloid of aspect ratio 2.0 in a web submitted to combined bending and shear is in good agreement with the observed values for hole-web depth ratios less than about .25.

2. The secondary bending theory appears to be conservative, at least as far as these experiments show, for those cases where the hole-web depth ratio is greater than about .30.

3. Actual values of maximum stress at the hole boundary are amenable to mathematical description.

The following recommendations are indicated by this thesis:

1. Further experimental investigations for hole-web depth ratios greater than .333.

2. Investigation of the stress distribution at the web edges in way of the hole. This may be accomplished with the photographs of model isochromatics included in the Original Data of this thesis (Appendix E). Results could be compared with secondary bending theory prediotions.

3. Further experimental investigations of ovaloids of

aspect ratio other than 2.0 -- particularly, 1.5.* A valuable simplified expression for the prediction of maximum stress at the hole and web boundaries could thus be deduced including all three variable parameters: hole-web depth ratio, shear-bending stress ratio, and aspect ratio.

---

* See p.15, Ref.(6).

INTRODUCTION

Ovaloid holes are frequently cut in structural webs for the purpose of reducing redundant weight or passing various piping, ventilation, electrical, or even access systems. It is desirable that the stresses be known at the boundary of these ovaloids if the structure is to incorporate the desired optimum safety factor.

Kirsch[7] and Tuzi[11] have investigated the effect on web stress distribution of ovaloids of aspect ratio 1.0 (circles) for hole-web depth ratios of zero in a uniform tension field and in pure bending, respectively; Howland and Stevenson[3] performed these investigations for hole-web depth ratios greater than zero and introduced an analysis for combined bending and shear. Durelli and Murray[13] have modified Kirsch's equations for two-dimensional stress systems and experimentally verified them. Neuber,[10] Inglis[4] and Wolf[12] have analyzed the stress distribution due to ellipses in webs in pure bending, a uniform tension field and combined shear and bending, respectively; Durelli and Murray[14] have extended and experimentally verified the first two cases. Greenspan[1] and Joseph and Brook[5] have performed analyses for the ovaloid in a web subjected to a uniform tension field and pure bending, respectively; Heller, Karl and Gerich[6] have experimentally examined the

---

*Numbers in brackets refer to Appendix F (Bibliography).

latter solution. Montgomery has investigated the applicability of the secondary bending analysis to an ovaloid of aspect ratio 2.0 and hole-web depth ratio 1.50 subjected to combined bending and shear with and without reinforcement. Heller has analyzed the stress distribution at the boundary of ovaloids (both major and minor axes vertical) and squares in webs of finite depth subjected to combined bending and shear (see Appendix A-I). This thesis will investigate by photoelastic methods the stress distribution at the boundary of an ovaloid of aspect ratio 2.0 in webs of various depths subjected to combined bending and shear and simultaneously seek to verify the applicability of the secondary bending theory (commonly used in practice) and Heller's solution.

PROCEDURE

The model and a tensile test specimen were prepared from a single sheet of one-quarter-inch Catalin 61-893. Accepted details of procedure for the preparation of photoelastic models as outlined by Frocht and Murray were observed; accordingly edge and surface irregularities and machining stresses were minimized.

The material fringe constant was determined by a series of runs performed on the tensile test specimen. (See Fig. XXXIV-B.) Equipment for the support of and application of loadings to the model was built and arranged as shown in Fig. I. With this equipment it was theoretically possible to subject the model to ratios of shear to bending moment varying from zero to infinity. Actually, ratios between 0 and 1 were used, since accuracy falls off rapidly at higher ratios.

Five groups of runs were performed for values of hole-web ratios from 0.100 to 0.333; these variations were accomplished by successive reductions of the web height - hole size was maintained constant. Particular attention was devoted during machining to minimize any eccentricity of the hole in relation to the web edges. An aspect ratio of the ovaloid of 2.0 was selected as representative of current structural practice. The ovaloid was located at a point in the web sufficiently well removed (in accordance with

St. Venant's Principle) from any points of load application or support to preclude extraneous stress distortion at the hole.

In order to obtain a greater degree of accuracy in the determination of fringe order magnitudes at the hole boundary in the subsequent stress distribution analysis, loadings were maximized during the variation of shear to bending stress ratio to obtain the largest possible number of fringe orders, care being taken not to exceed the yield point of the material (about fifteen fringes) at any point in the model (generally at the web edge fillets). Care was taken during the application of loads to prevent a torsional or lateral bending of the model due to lateral load eccentricities. The small ball-bearing pulley used in conjunction with the upward loading of the model possessed a frictional restraint that was a negligible percentage of the load applied. The weight and moment of the web extension arm were taken into account. The polariscope and camera of the photoelasticity laboratory of the Department of Mechanical Engineering were used with a mercury vapor light source and Wratten filters #77A and #58 giving a light wave length of 5641 Å.

Each group of runs at constant hole-web depth ratio included a no-load photograph and five or six photographs of the web isochromatics at various values of shear-bending stress ratios. The analyzers were positioned for a dark

FIGURE I

TEST SET-UP

field. The time edge effect at the web edges was minimized by conducting the runs soon after machining - but allowing time enough for machining stresses to dissipate. Two annealings were necessary (prior to the runs for b/c of .125 and .250) to minimize the time-edge effect at the hole boundary.

RESULTS

The stress distributions at the boundary of a given ovaloid hole of aspect ratio 2.0 in a web of varying depth subjected to various ratios of shear to bending stress are presented in Figures II-XXVIII. The ordinates are in dimensionless form - $\frac{\sigma}{\sigma_0}$. (Refer to Table I of Appendix C.) Three distributions are included in each plot: observed stress and stress predicted by the secondary bending theory and Heller's analysis. The variation in the shear to bending stress ratio ($\frac{\tau}{\sigma}$) is plotted at the top of each figure.

The maximum stress at the boundary of the same given ovaloid at various web depths for varying values of shear to bending stress as obtained from Figures II-XXVIII are depicted in Figures XXIX-XXXIII. Observed and predicted values are included.

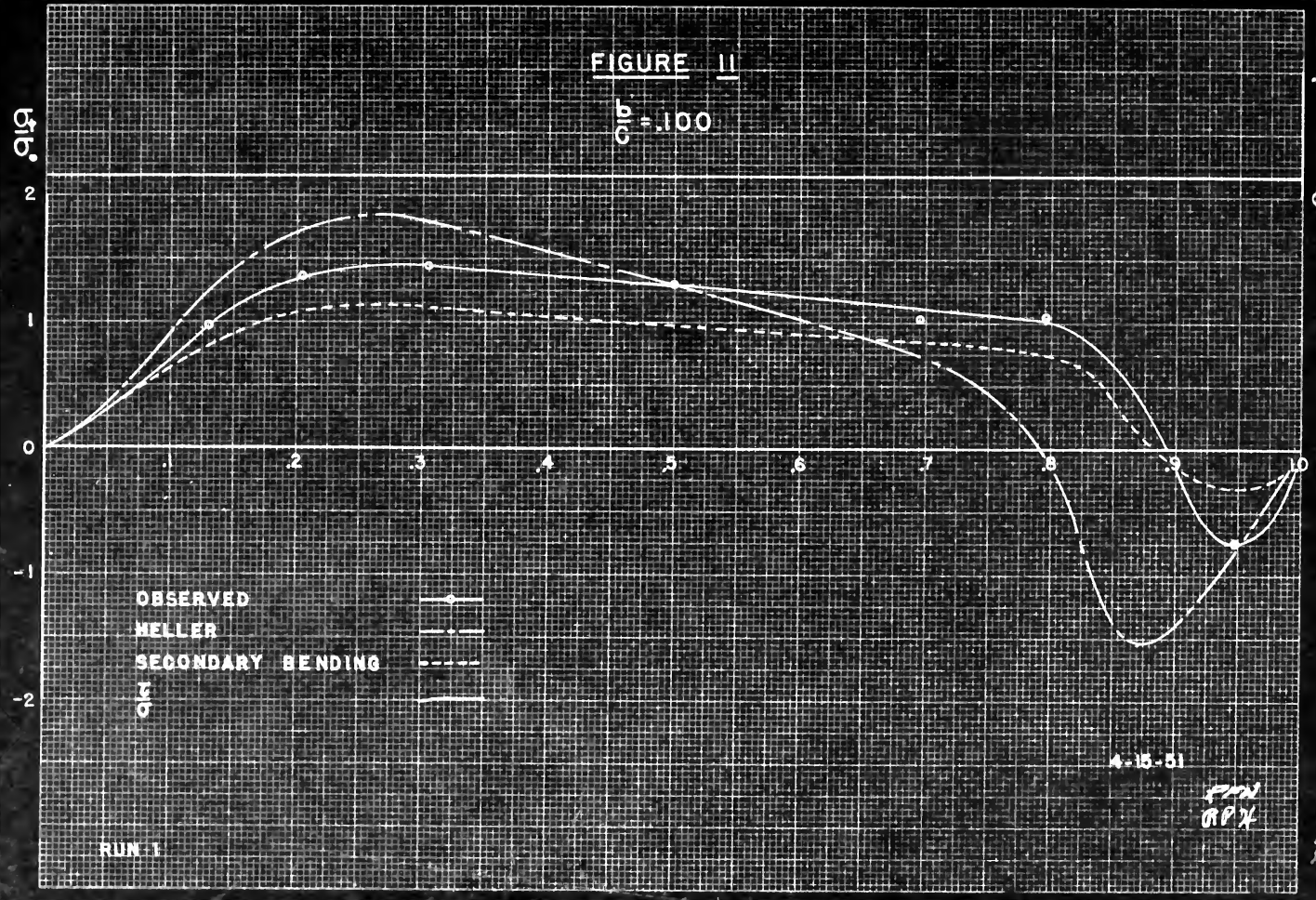
FIGURE 11
$\frac{c_{1b}}{c_{1b}} = .100$
σ_{1b}
2
1
0
-1
-2
.1
.2
.3
.4
.5
.6
.7
.8
.9
1.0
OBSERVED
HELLER
SECONDARY BENDING
$\frac{x}{c}$
4-15-51
RUN 1

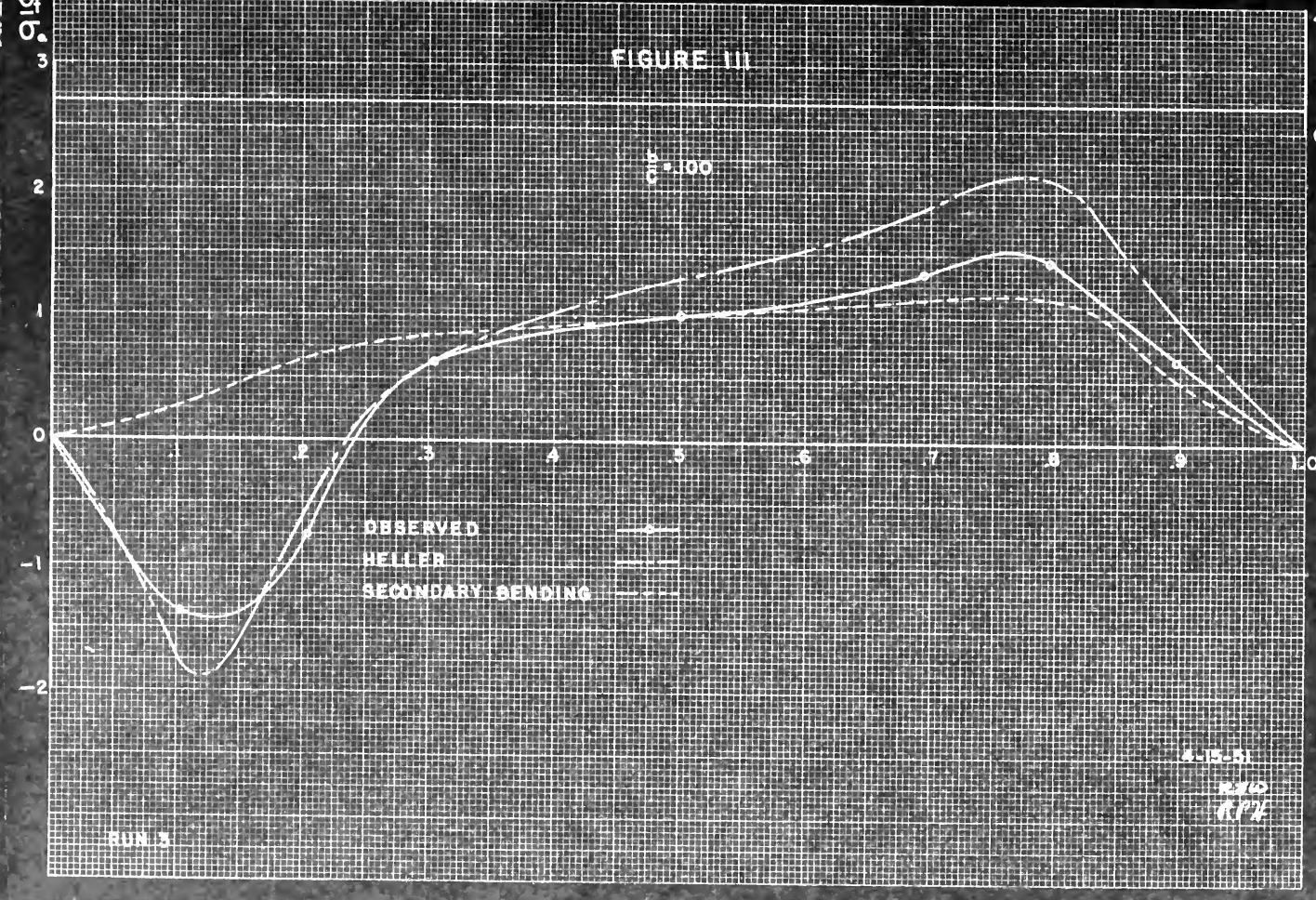
FIGURE 11
$\frac{b}{c}$ = 100
3
2
1
0
−1
−2
.1
.2
.3
.4
.5
.6
.7
.8
.9
1.0
OBSERVED
HELLER
SECONDARY BENDING
4-15-31
RUN 3

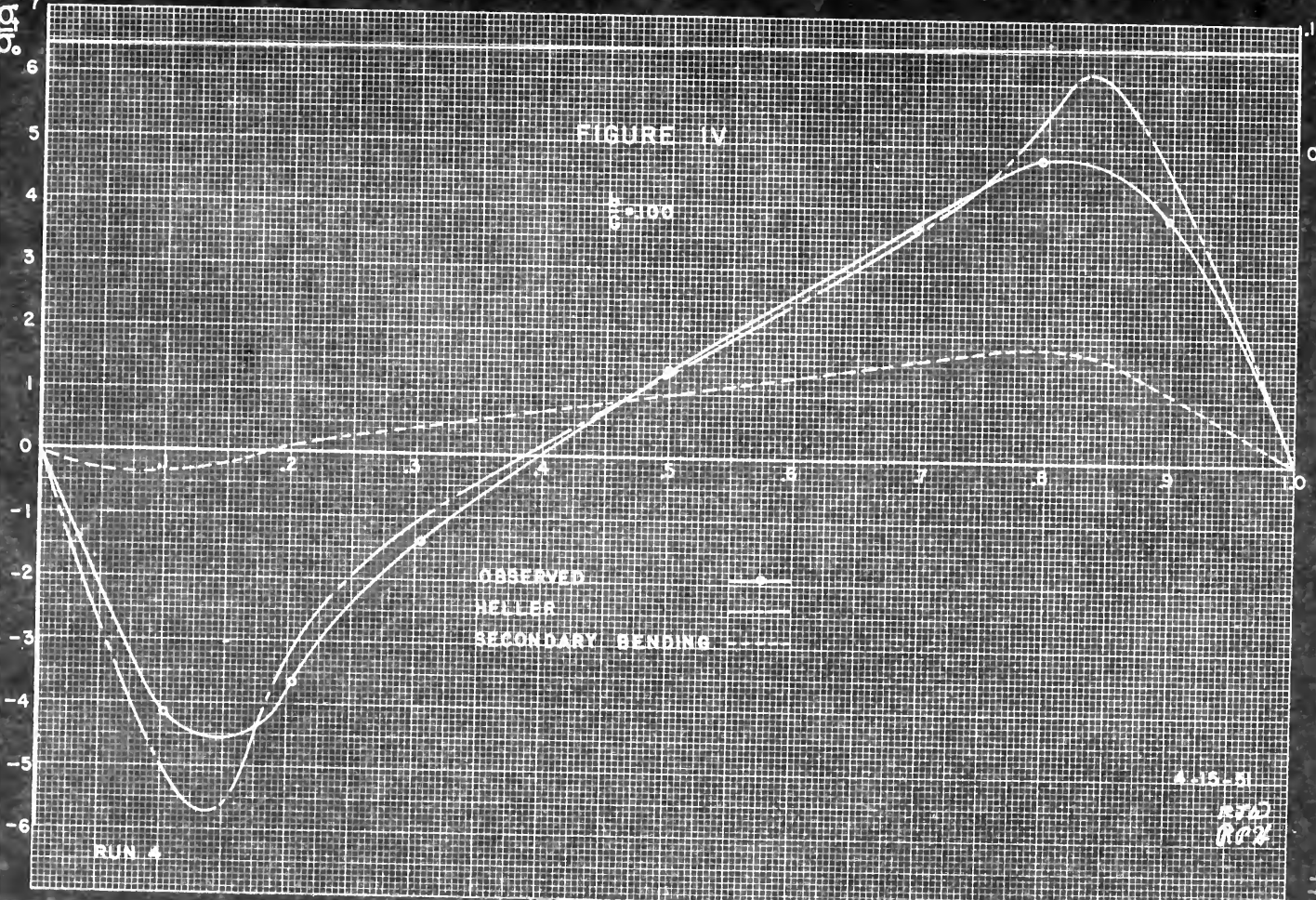
FIGURE IV
$\frac{R}{R_0}$=100
OBSERVED
HELLER
SECONDARY BENDING
RUN 4

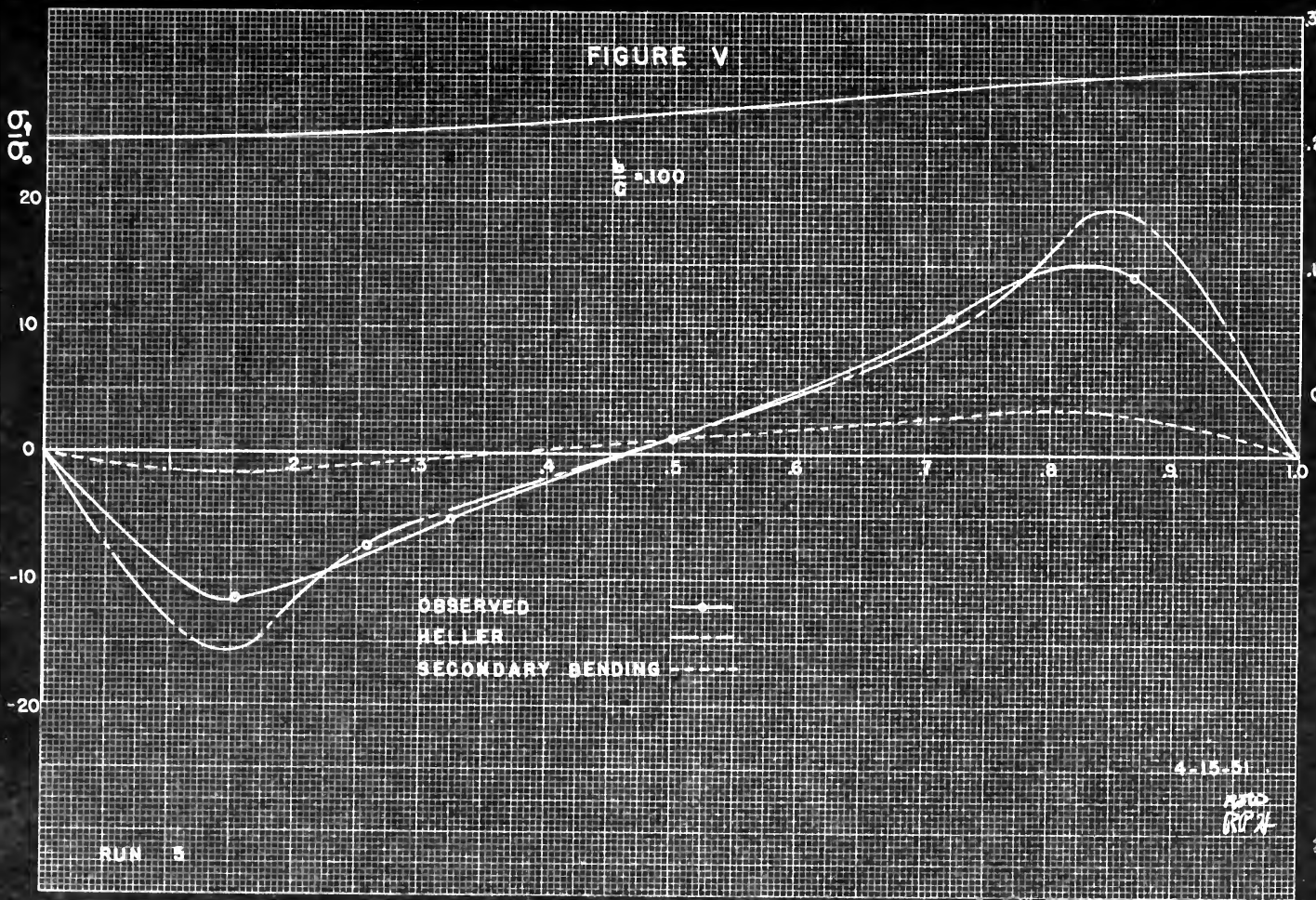
FIGURE V
σ/q
20
10
0
-10
-20
.1
.2
.3
.4
.5
.6
.7
.8
.9
1.0
OBSERVED
HELLER
SECONDARY BENDING
4-15-51
RUN 5

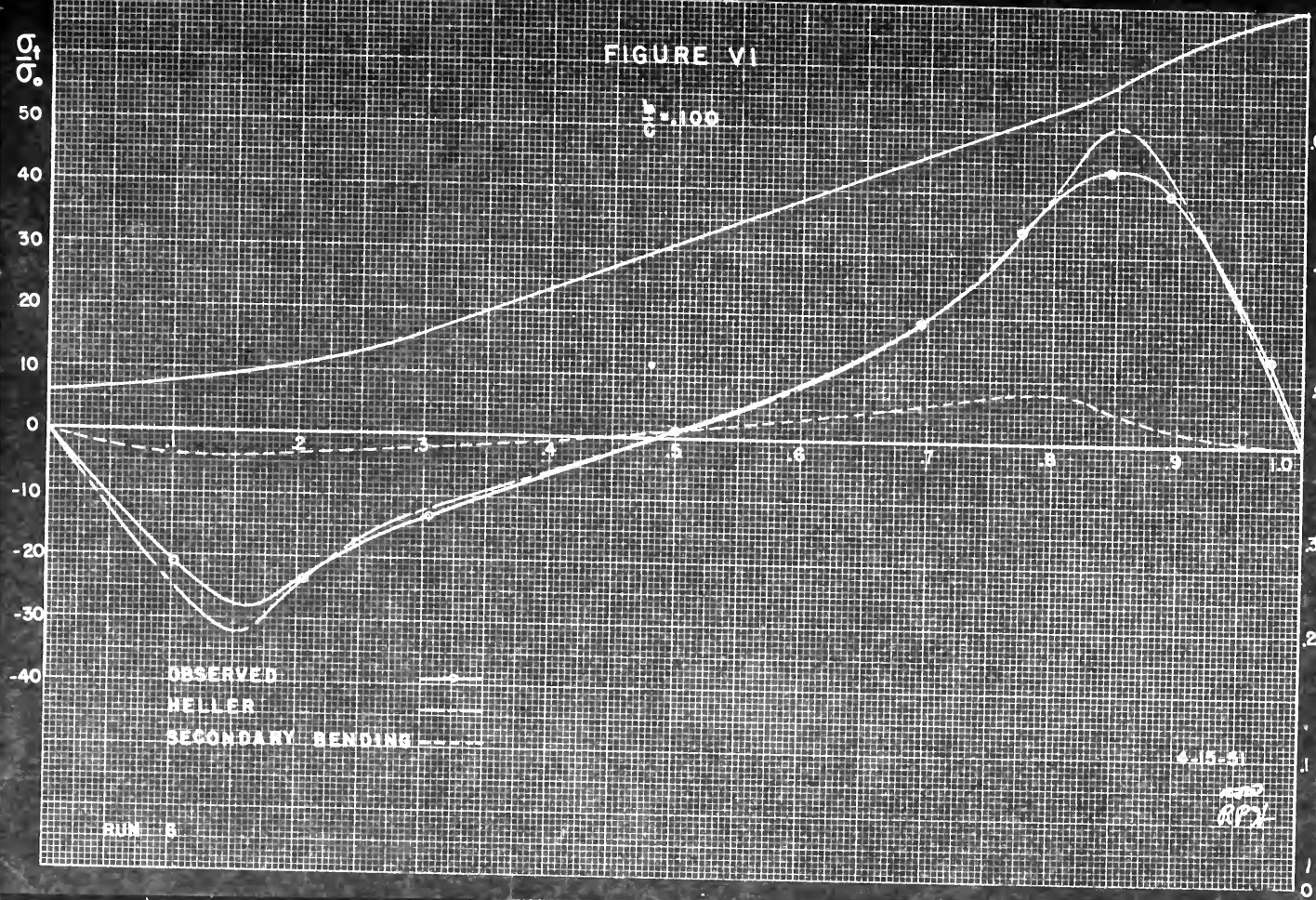
FIGURE VI
$\frac{h}{c} = .100$
σ/σ_o
50
40
30
20
10
0
-10
-20
-30
-40
1
2
3
4
5
6
7
8
9
10
OBSERVED
HELLER
SECONDARY BENDING
RUN 5
.4
.3
.2
.1
0

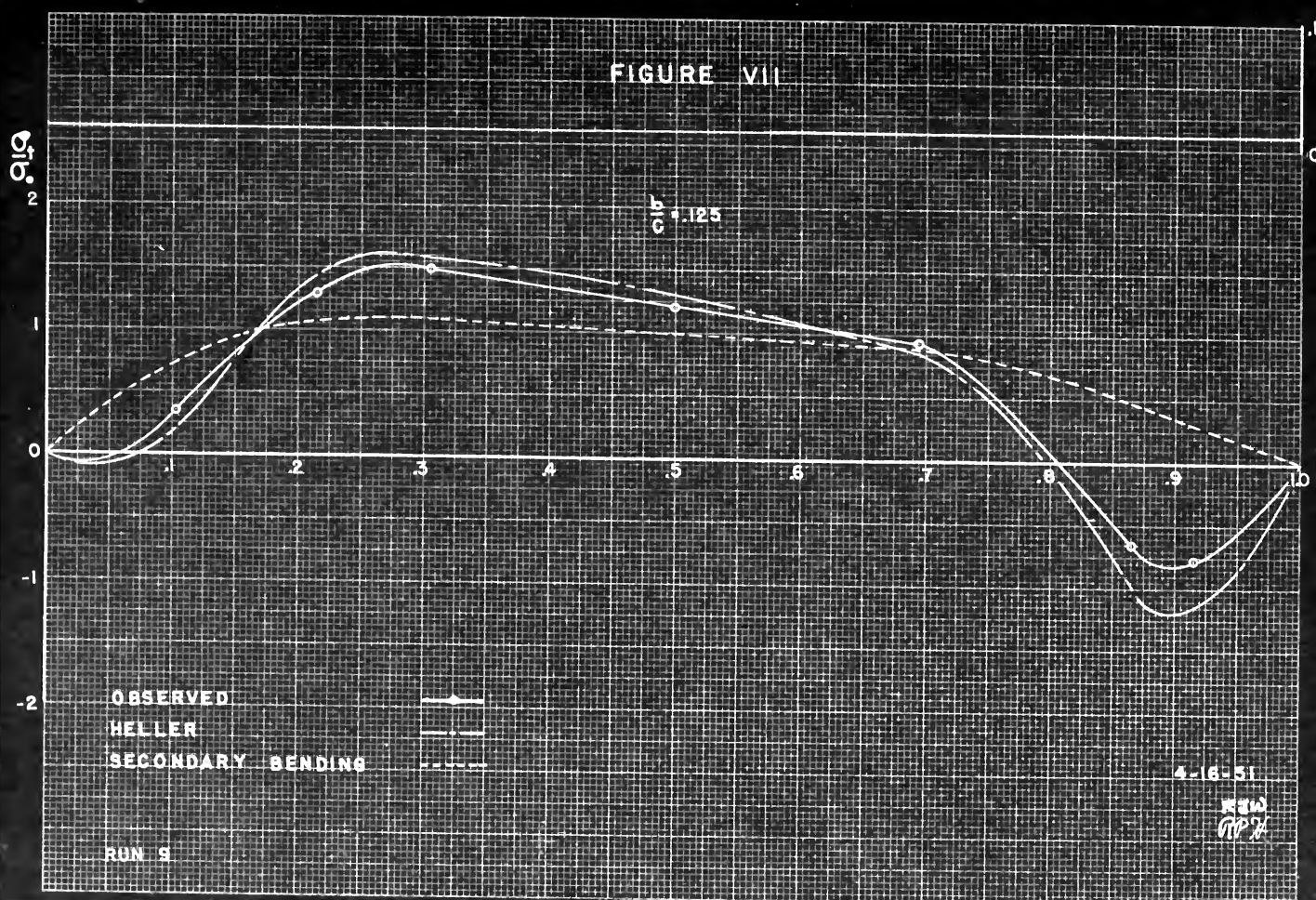
FIGURE VII
c_{l_p}
C = 1.125
2
1
0
-1
-2
.1
.2
.3
.4
.5
.6
.7
.8
.9
1.0
OBSERVED
HELLER
SECONDARY BENDING
RUN 9
4-16-51

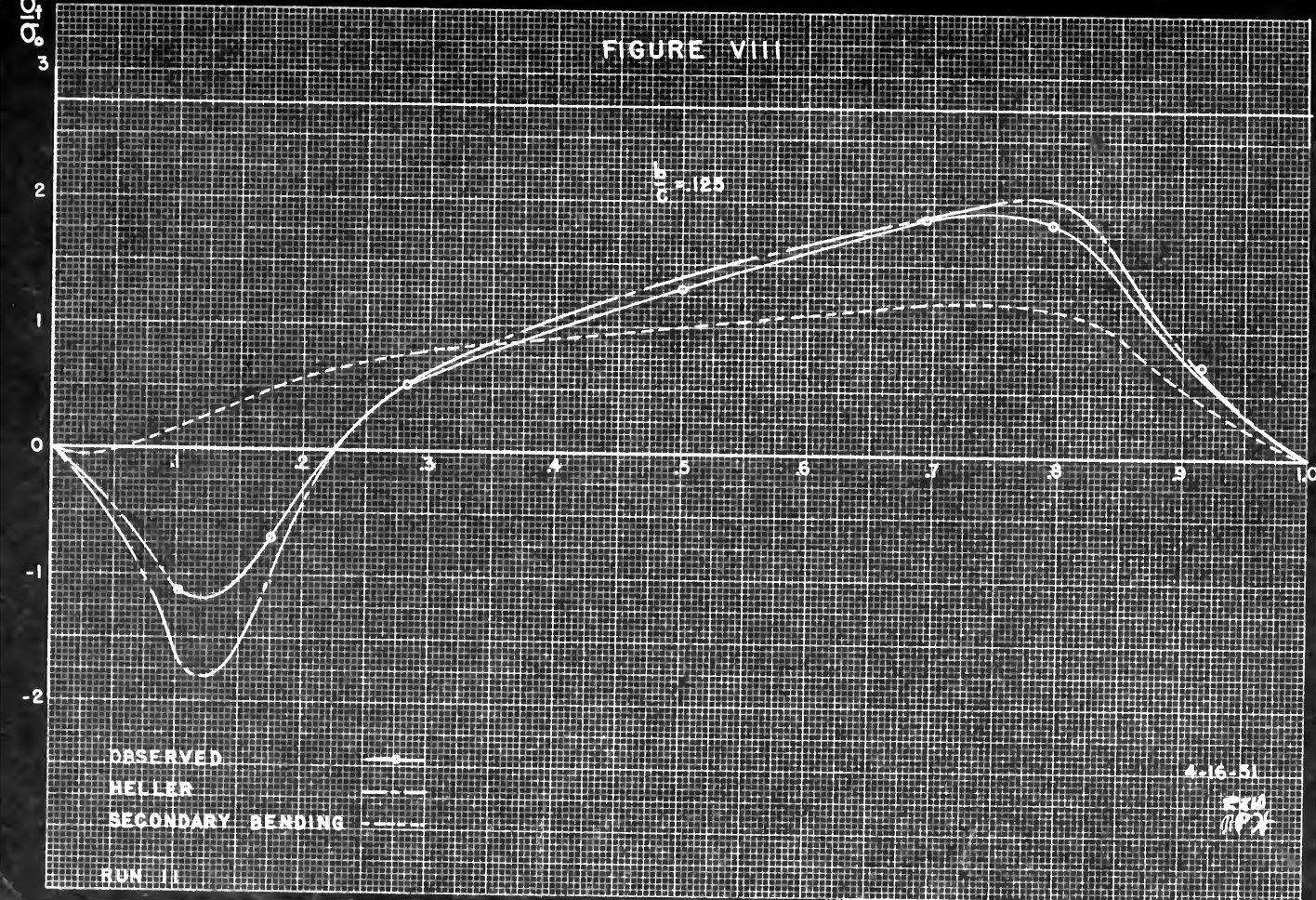
FIGURE VIII
$\frac{b}{c}$ = 12.5
3
2
1
0
-1
-2
.1
.2
.3
.4
.5
.6
.7
.8
.9
1.0
OBSERVED
HELLER
SECONDARY BENDING
RUN 11
4-16-51

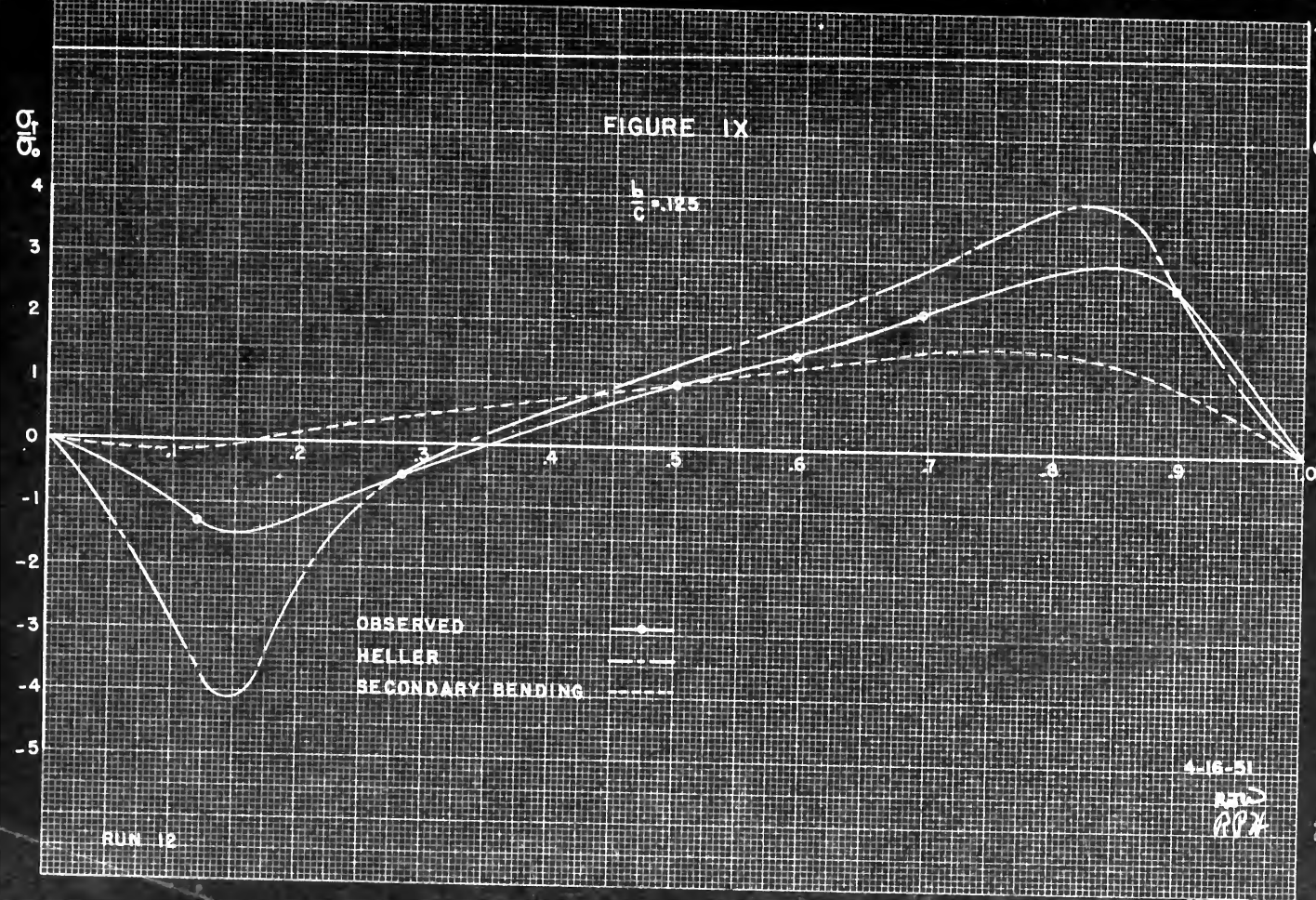
FIGURE IX
$\frac{b}{c}$ = .125
$\frac{\sigma_r}{\sigma_o}$
4
3
2
1
0
-1
-2
-3
-4
-5
.2
.3
.4
.5
.6
.7
.8
.9
1.0
OBSERVED
HELLER
SECONDARY BENDING
RUN 12

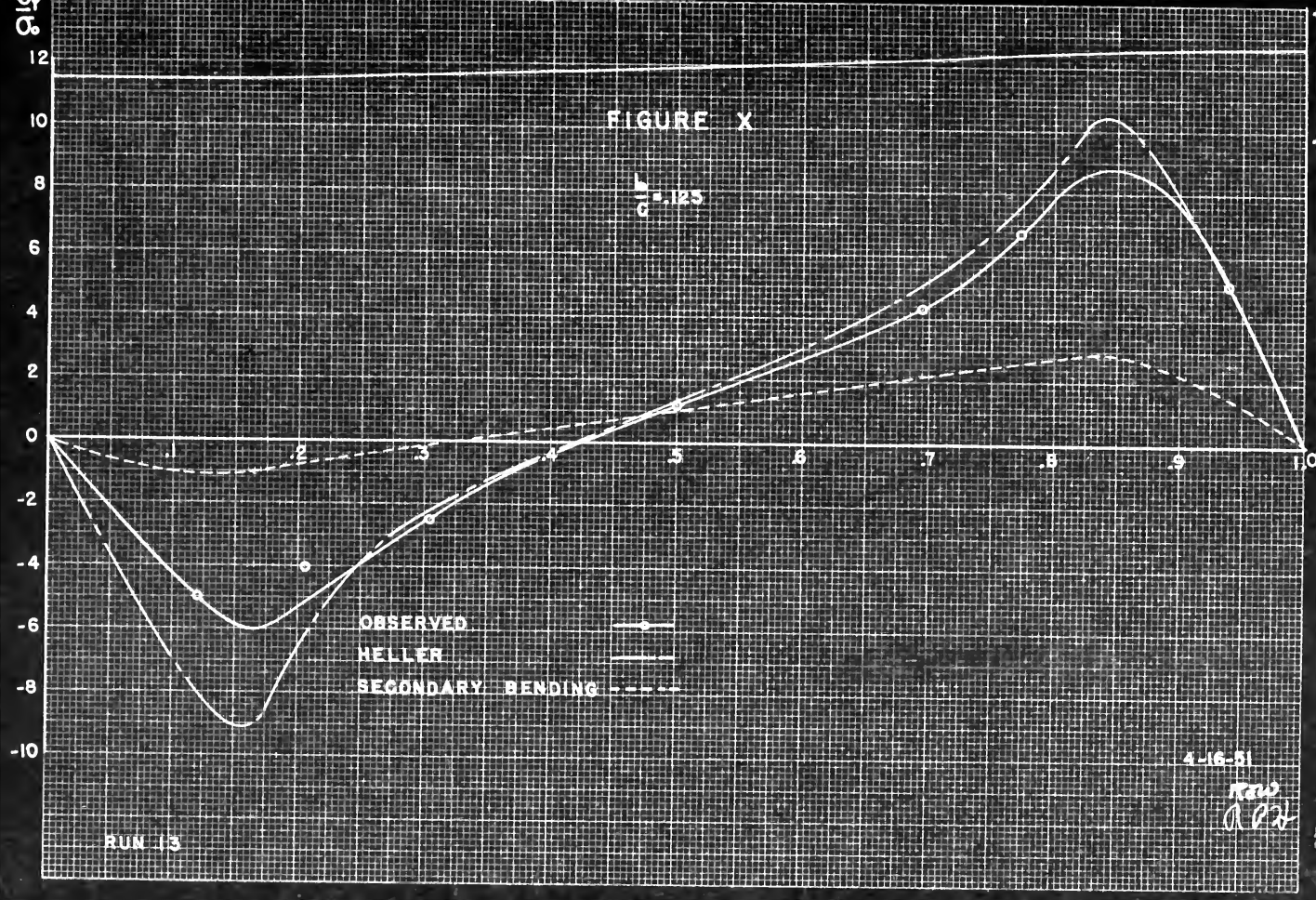
FIGURE X
b/c = .125
OBSERVED
HELLER
SECONDARY BENDING
RUN 13
4-16-51

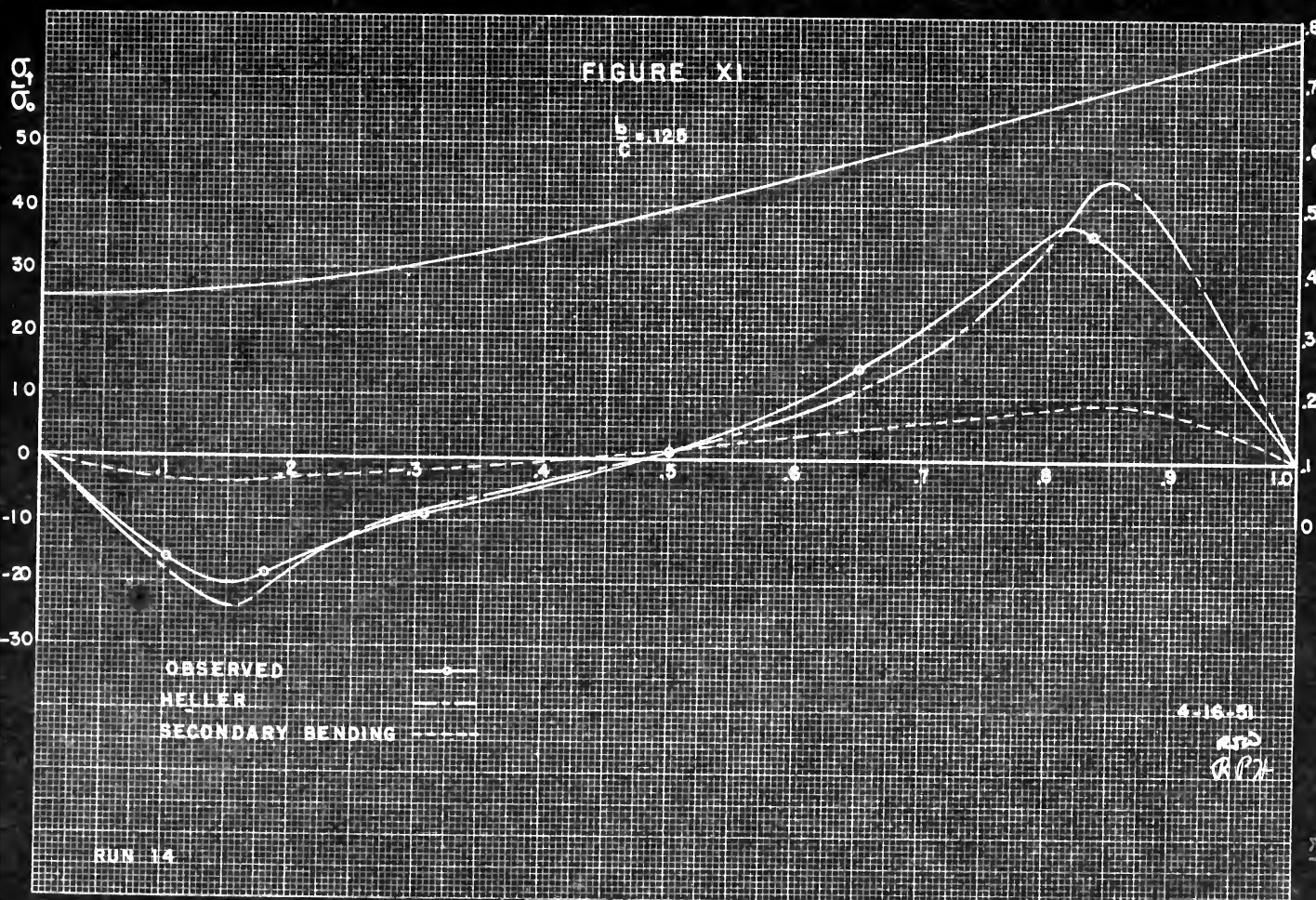
FIGURE XI
b/c = .125
σ/q
50
40
30
20
10
0
-10
-20
-30
.1
.2
.3
.4
.5
.6
.7
.8
.9
1.0
.6
.7
.5
.4
.3
.2
.1
0
OBSERVED
HELLER
SECONDARY BENDING
RUN 14
4-16-51

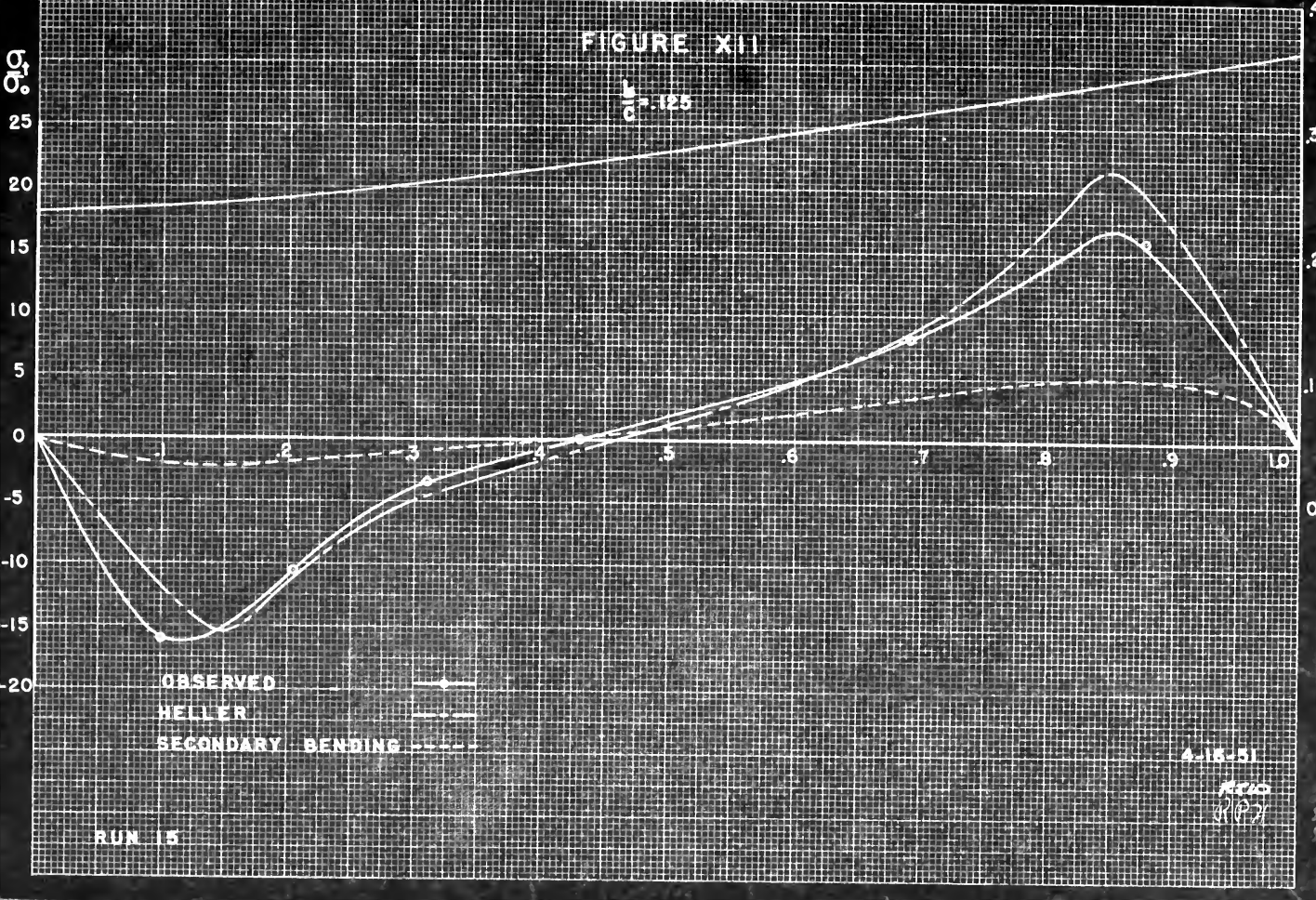
FIGURE XII
$\frac{h}{d}$=.125
$\frac{\sigma_t}{\sigma_o}$
25
20
15
10
5
0
-5
-10
-15
-20
.1
.2
.3
0
.1
.2
.3
.4
.5
.6
.7
.8
.9
1.0
OBSERVED
HEILER
SECONDARY BENDING
RUN 15

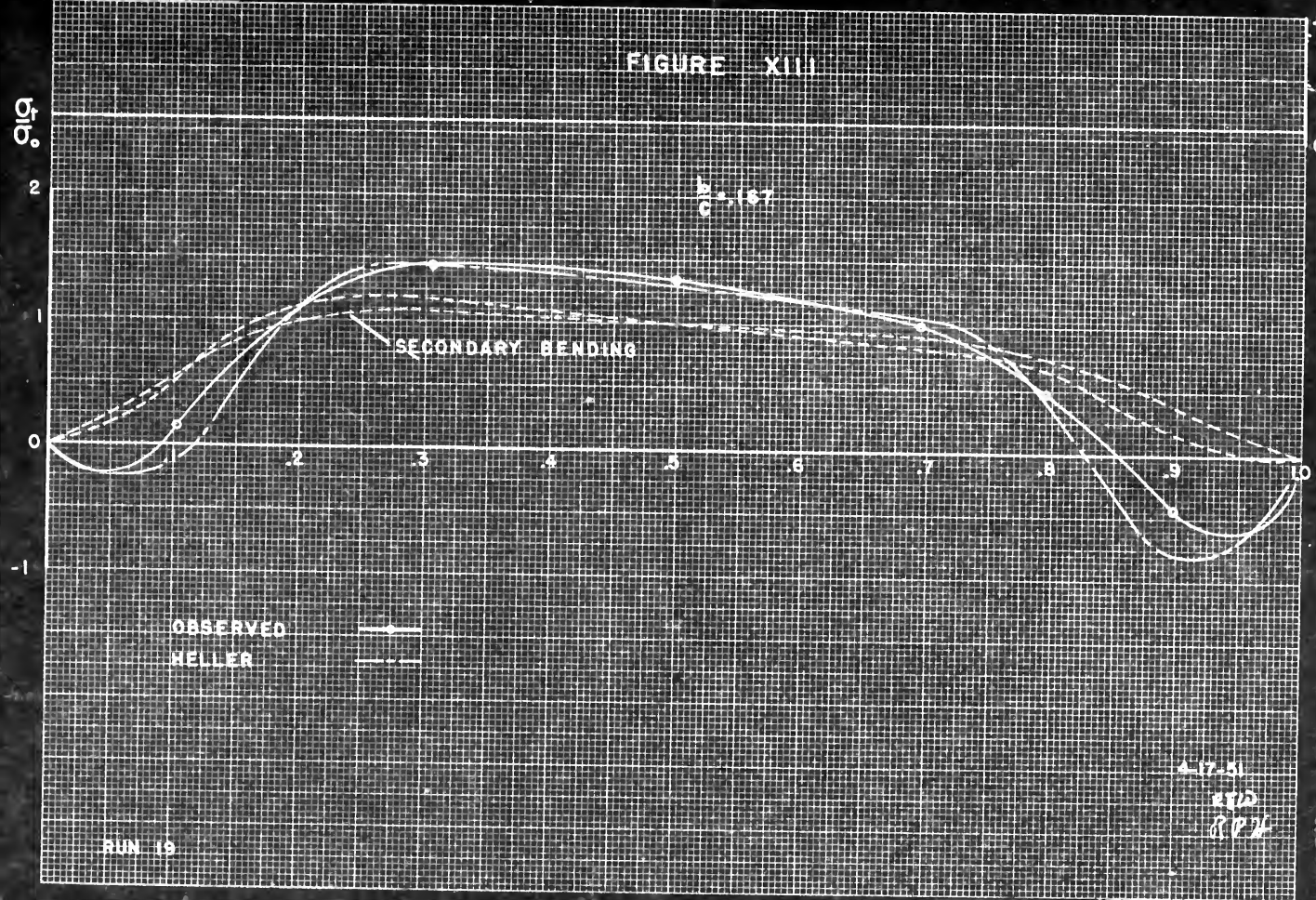
FIGURE XIII
$\frac{\sigma_t}{\sigma_o}$
2
1
0
-1
$\frac{b}{c}$ = .167
SECONDARY BENDING
.2
.3
.4
.5
.6
.7
.8
.9
1.0
OBSERVED
HELLER
RUN 19

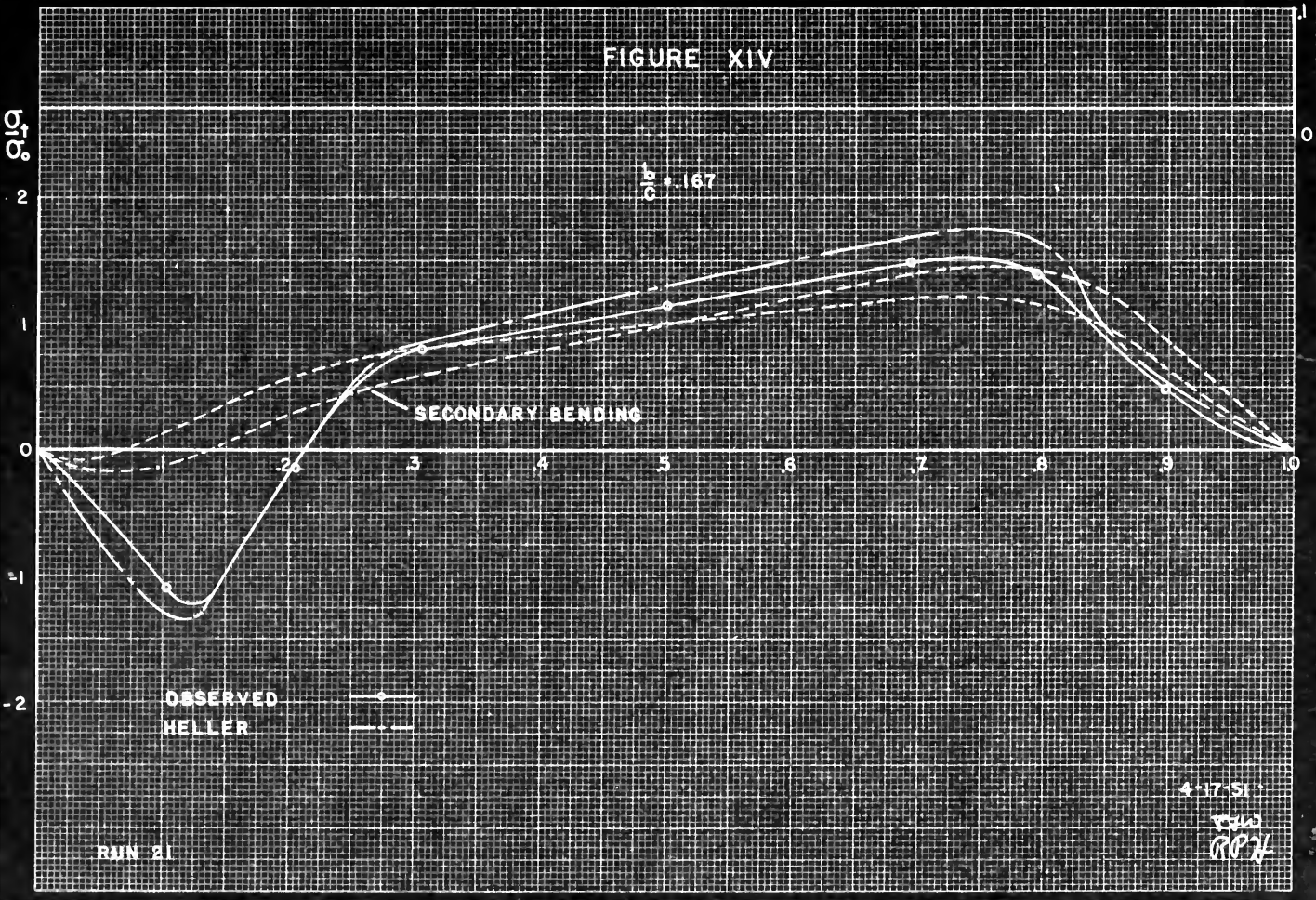
FIGURE XIV
$\frac{b}{c}$ = .167
SECONDARY BENDING
OBSERVED
HELLER
RUN 21
4-17-51

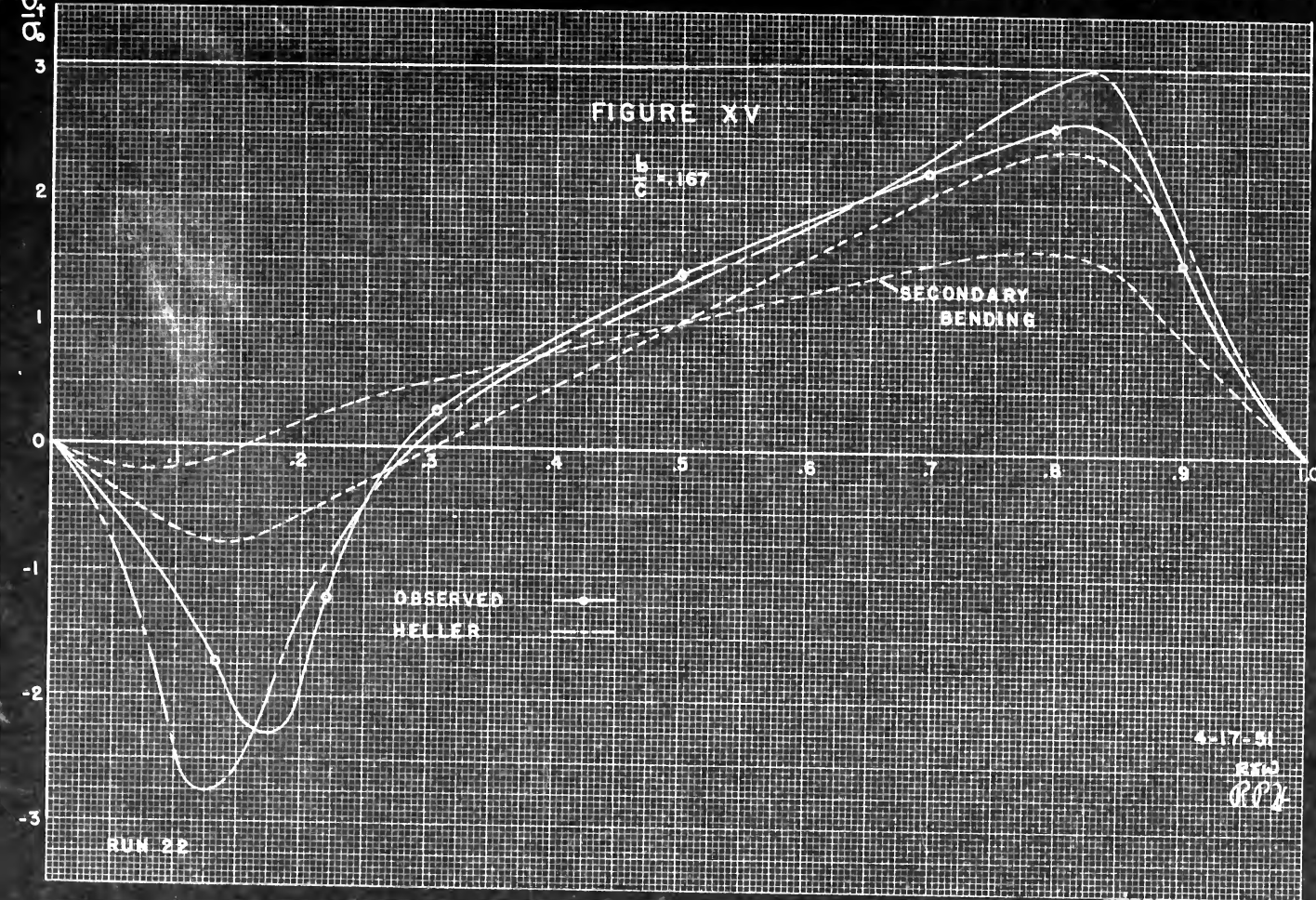
FIGURE XV
b/c = 1.167
SECONDARY BENDING
OBSERVED
HELLER
RUN 22
4-17-51
3
2
1
0
-1
-2
-3
.2
.3
.4
.5
.6
.7
.8
.9

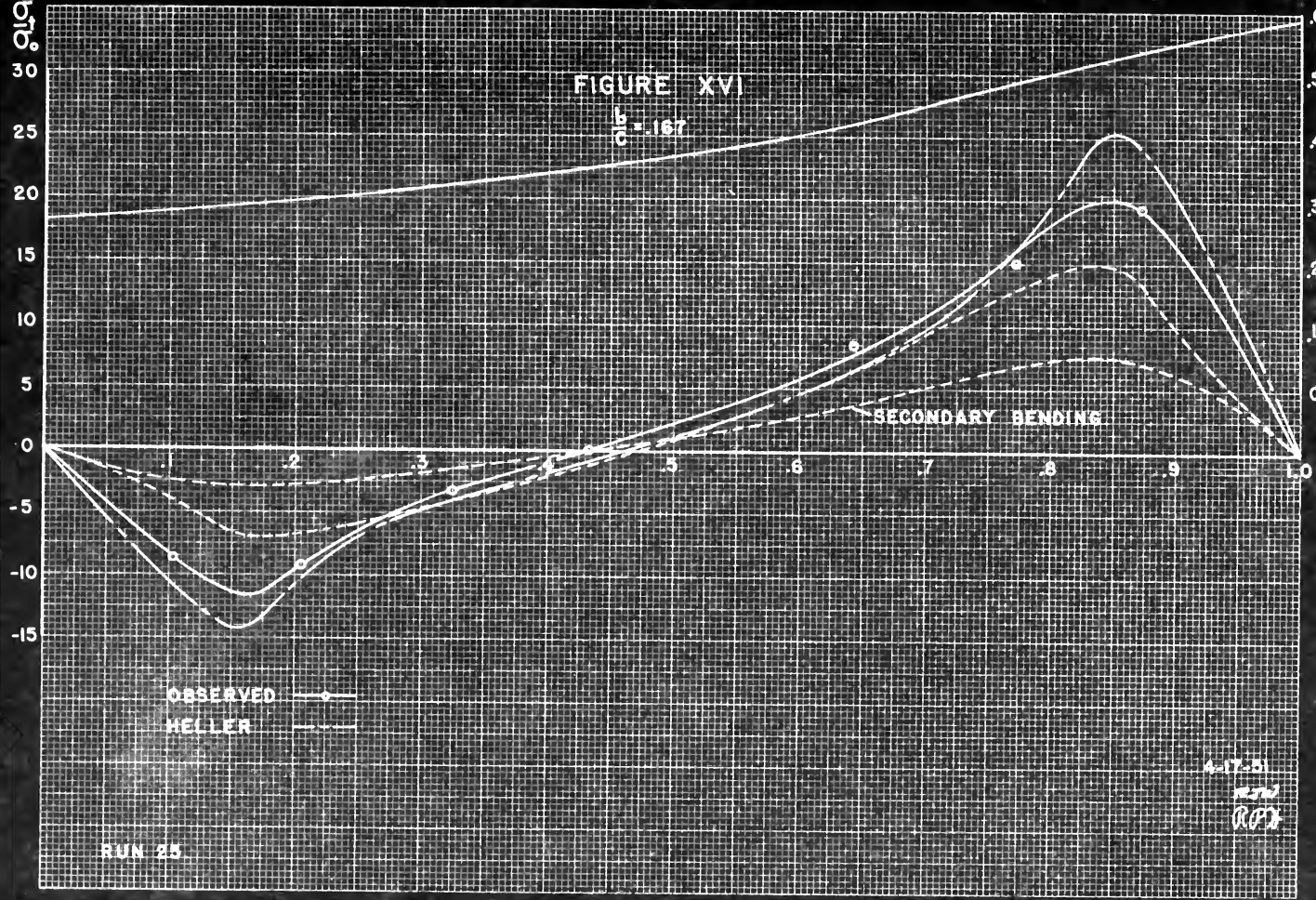
FIGURE XVI
b/c = .167
SECONDARY BENDING
OBSERVED
HELLER
RUN 25
30
25
20
15
10
5
0
-5
-10
-15
.1
.2
.3
.4
.5
.6
.7
.8
.9
1.0

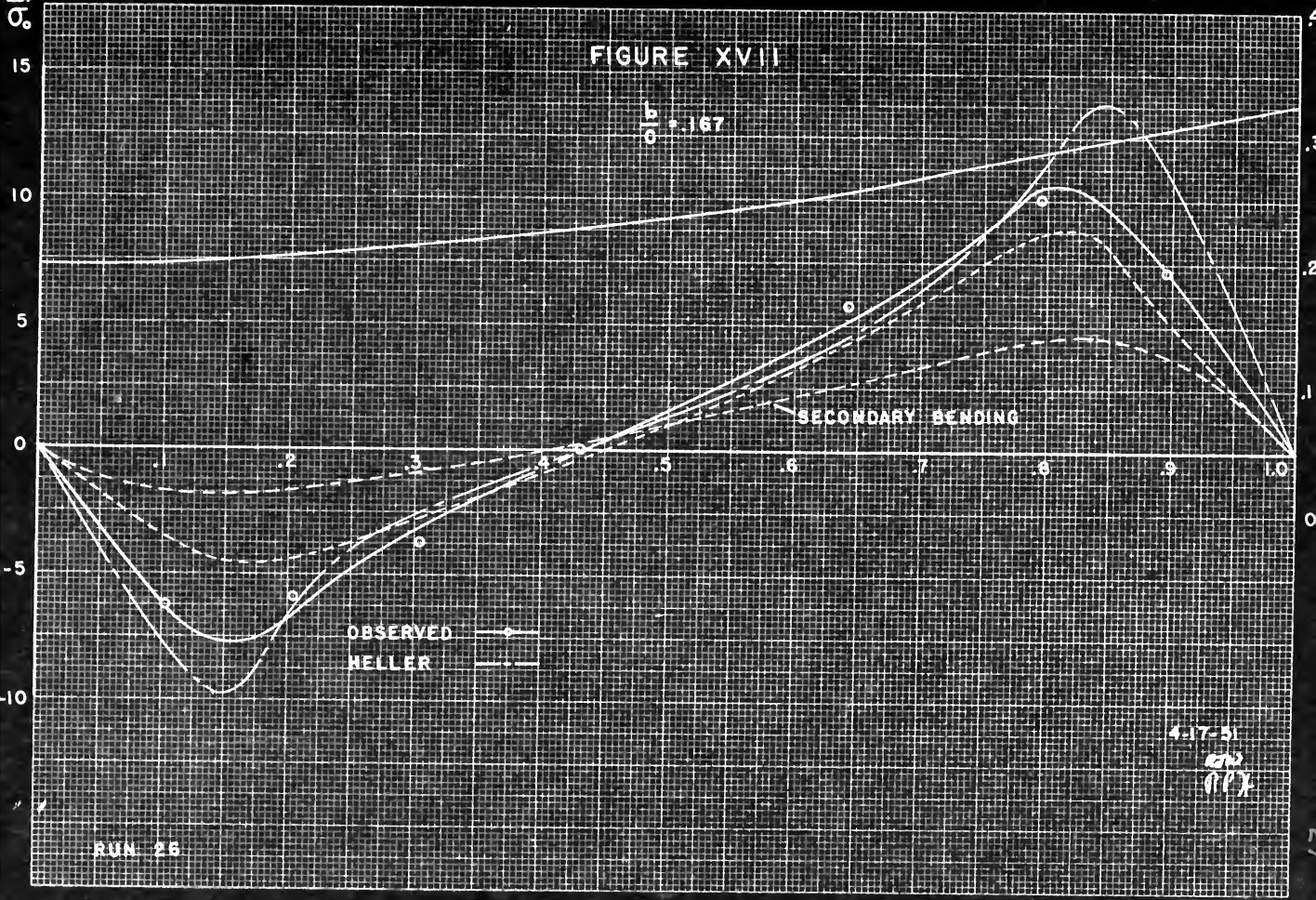
FIGURE XVII
$\frac{b}{D} = .167$
σ_o
15
10
5
0
-5
-10
.1
.2
.3
.4
.5
.6
.7
.8
.9
1.0
.3
.2
.1
0
SECONDARY BENDING
OBSERVED
HELLER
4-17-51
RUN 26

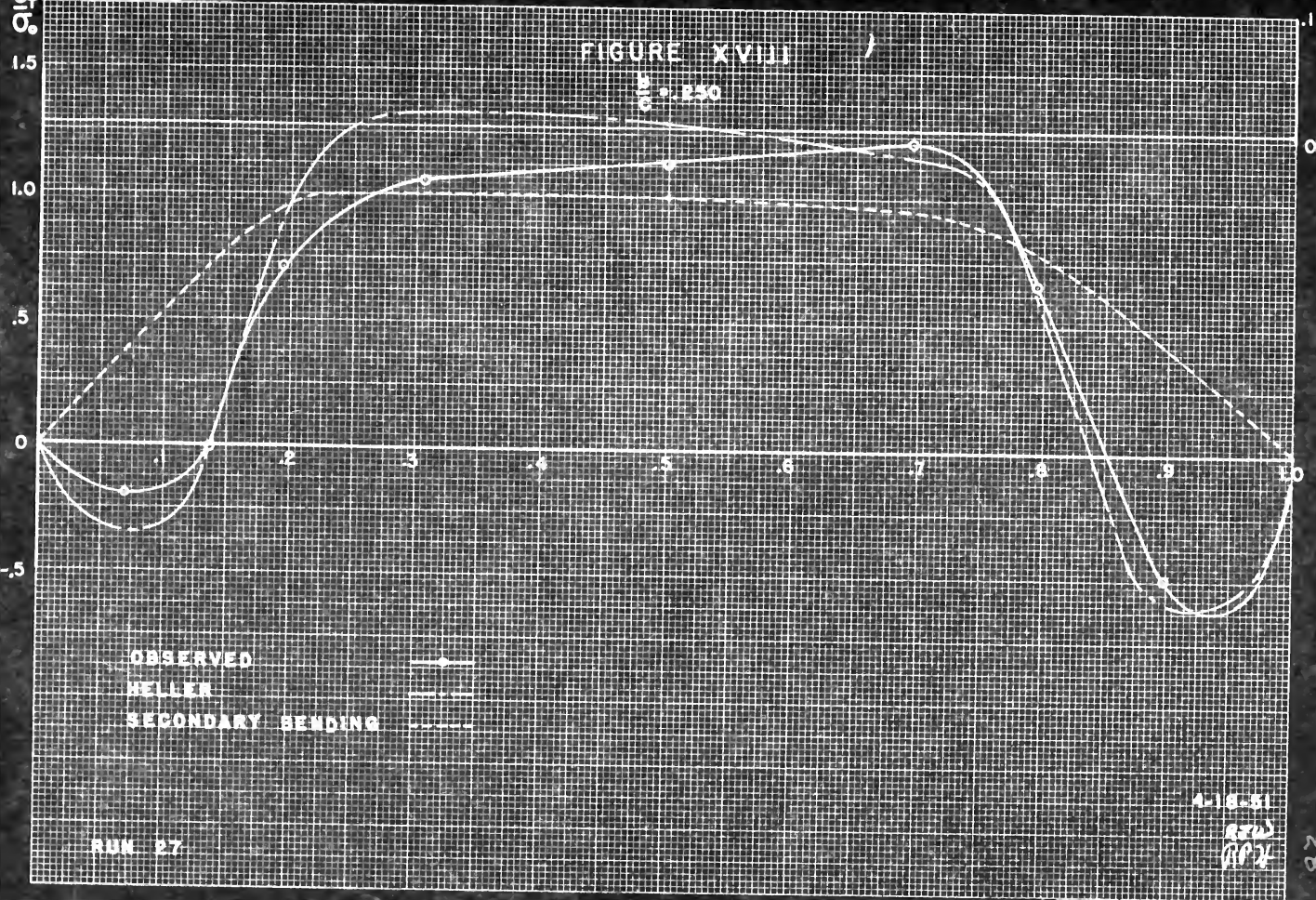
FIGURE XVIII
1.5
1.0
.5
0
-.5
.1
.2
.3
.4
.5
.6
.7
.8
.9
1.0
OBSERVED
HELLER
SECONDARY BENDING
RUN 27

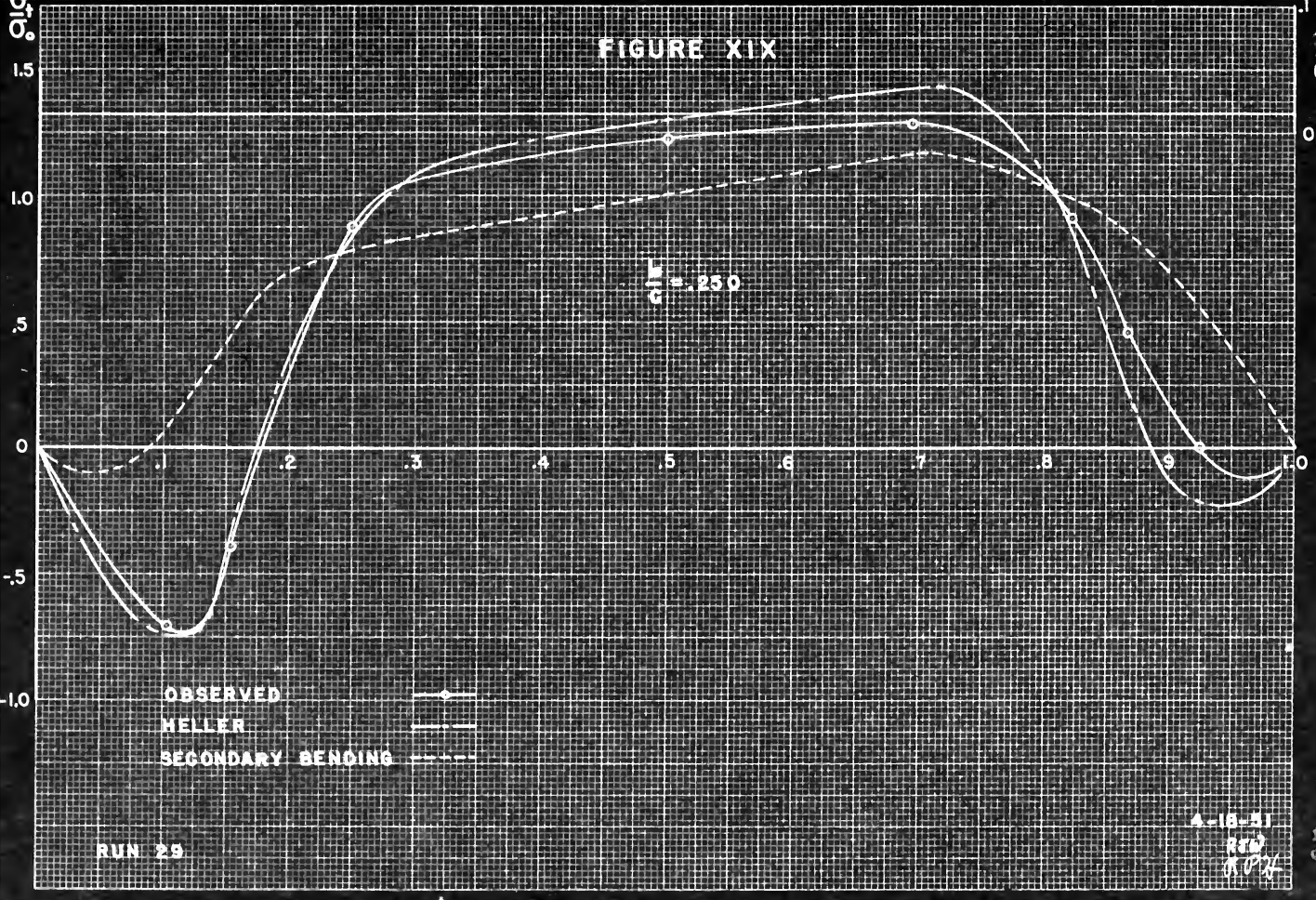
FIGURE XIX
1.5
1.0
.5
0
-.5
-1.0
.1
.2
.3
.4
.5
.6
.7
.8
.9
1.0
$\frac{h}{c}$ = .250
OBSERVED
HELLER
SECONDARY BENDING
RUN 29

FIGURE XX

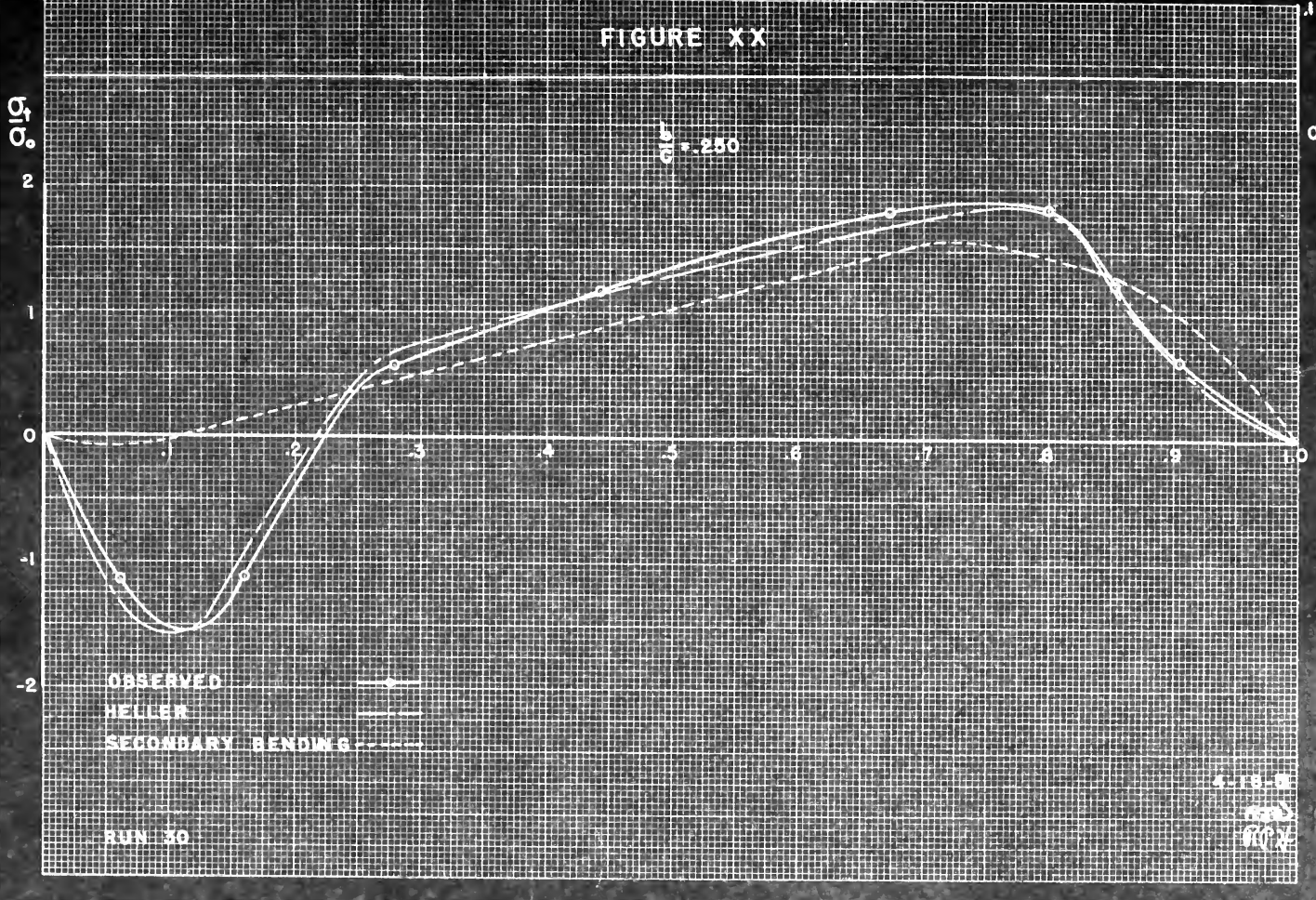
$\frac{\sigma_t}{\sigma_o}$
$\frac{h}{d}$ = .250
2
1
0
-1
-2
.1
.2
.3
.4
.5
.6
.7
.8
.9
1.0
OBSERVED
HELLER
SECONDARY BENDING
RUN 30

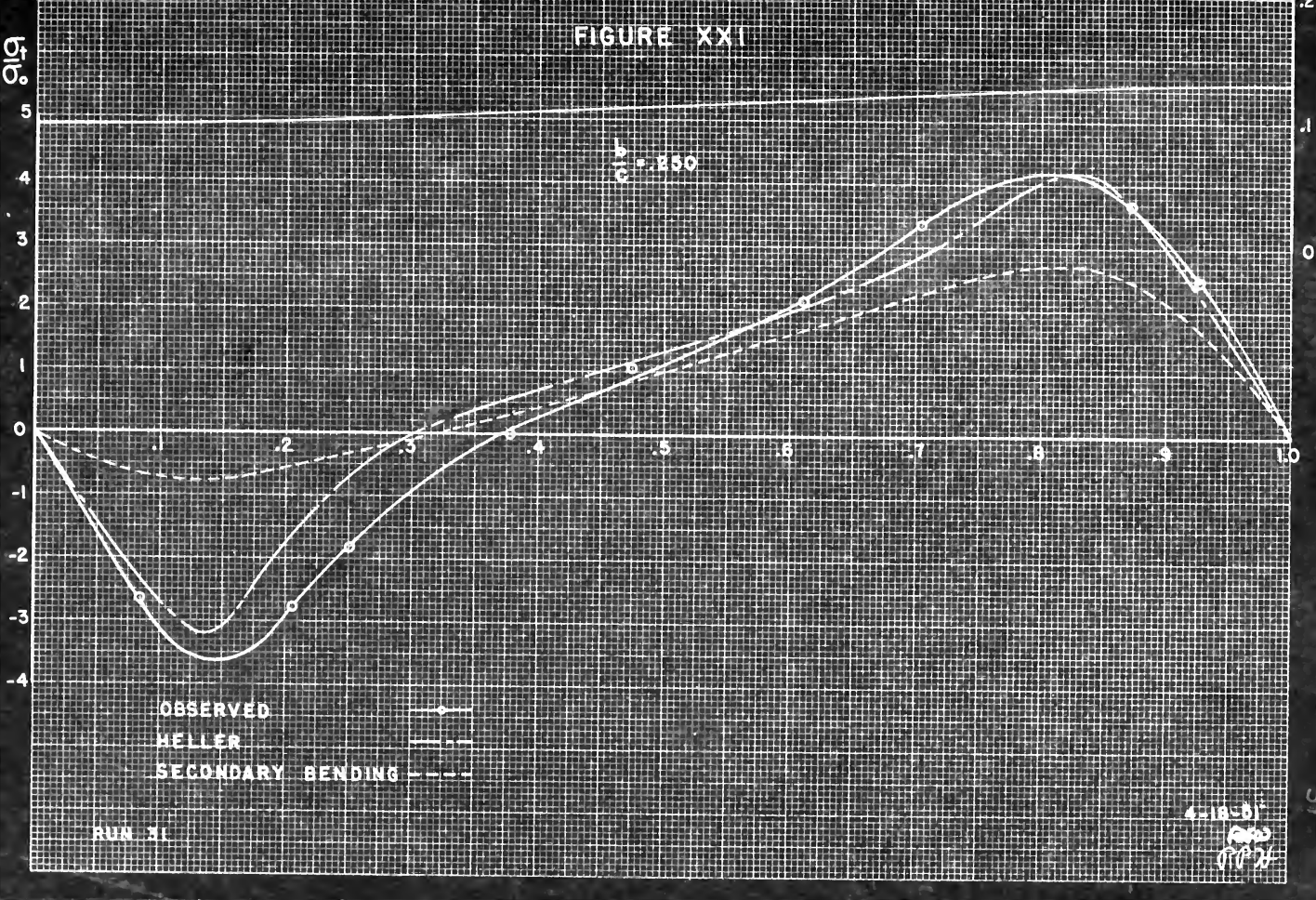
FIGURE XXI
$\frac{b}{c}$ = .850
OBSERVED
HELLER
SECONDARY BENDING
RUN 31
4-18-51

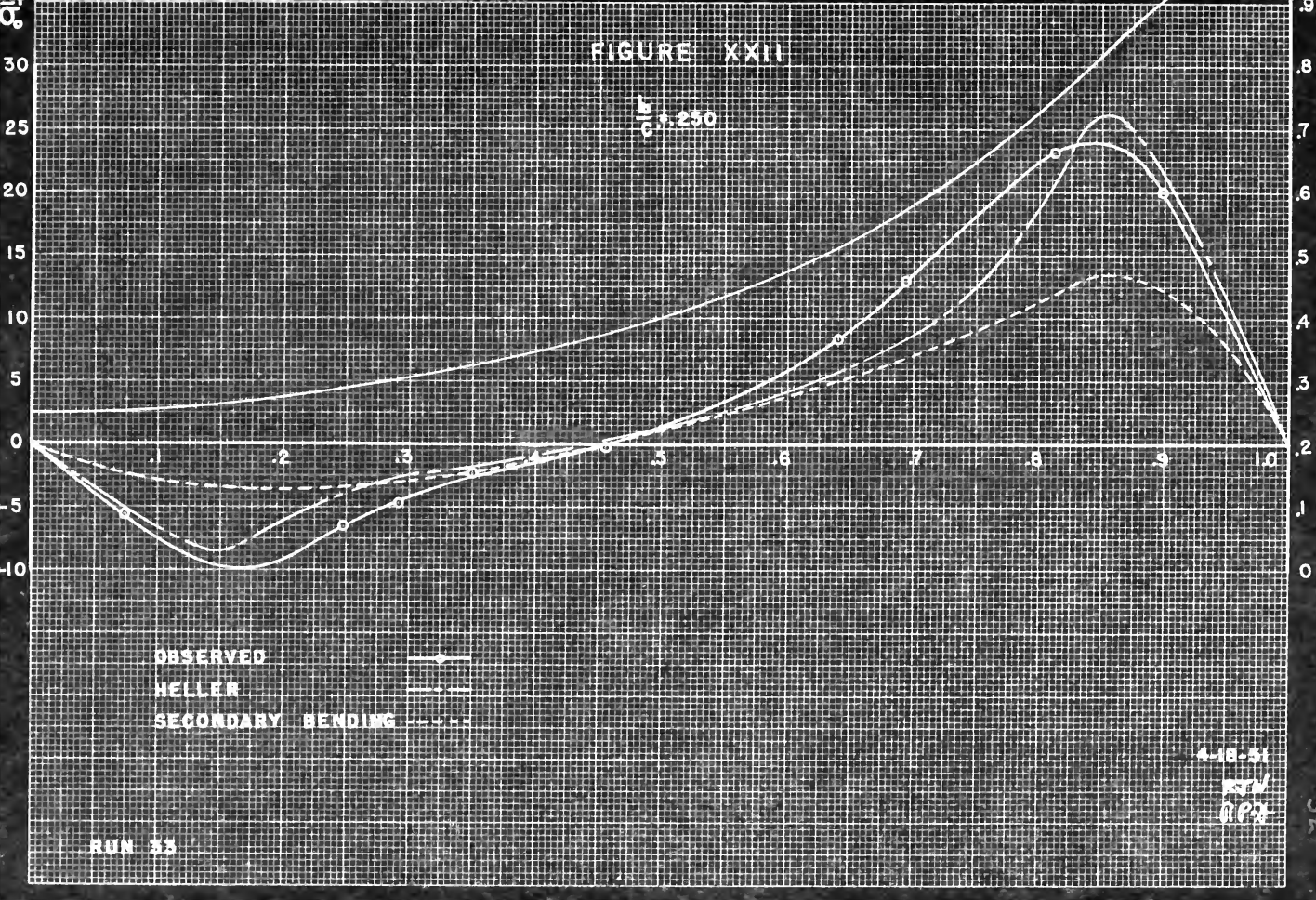
FIGURE XXII
$\frac{b}{c} = .250$
OBSERVED
HELLER
SECONDARY BENDING
RUN 35

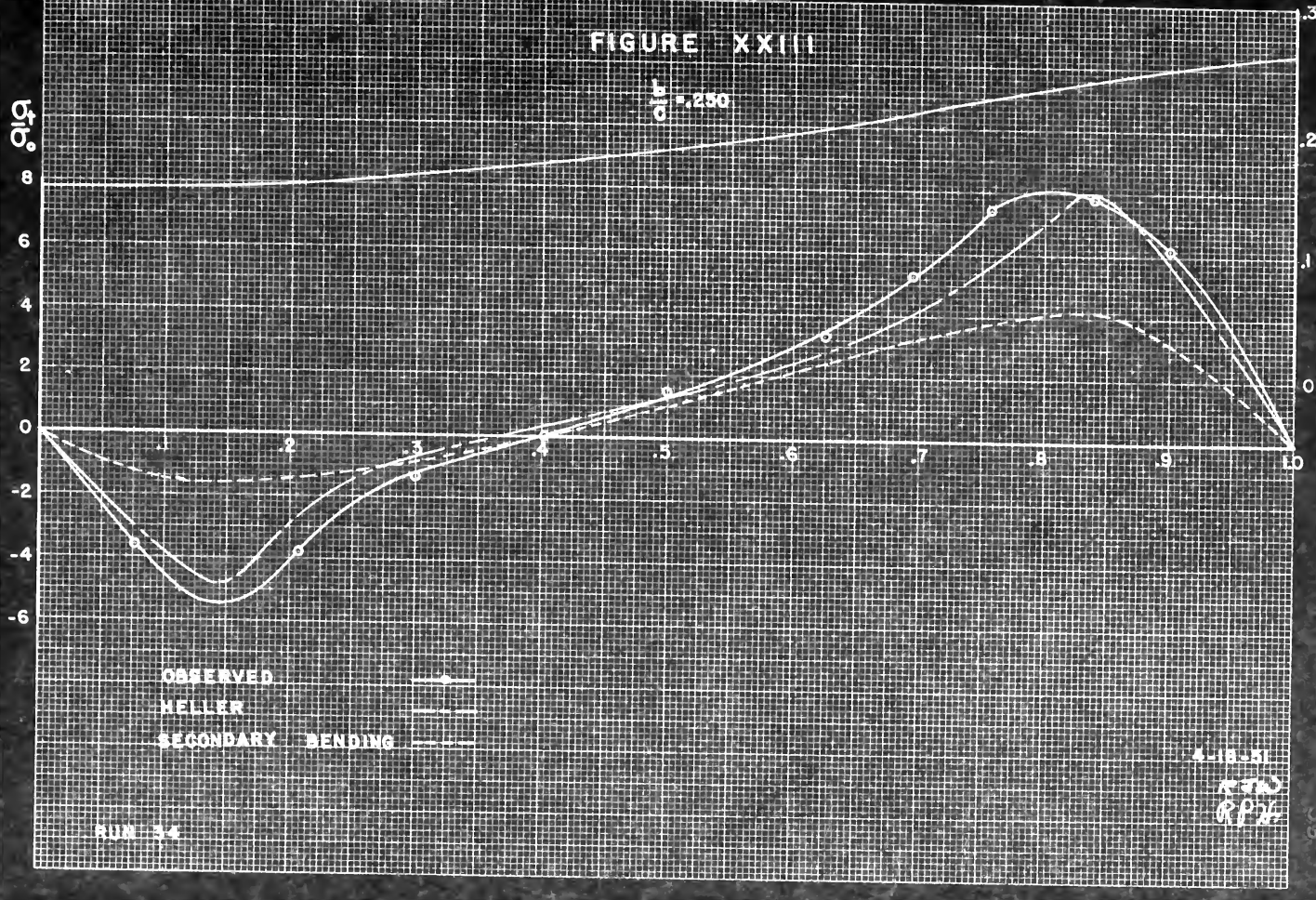
FIGURE XXIII
$\frac{b}{d}$ = .250
σ_t/σ_o
8
6
4
2
0
-2
-4
-6
.1
.2
.3
.4
.5
.6
.7
.8
.9
1.0
.3
.2
.1
0
OBSERVED
HELLER
SECONDARY BENDING
RUN 34

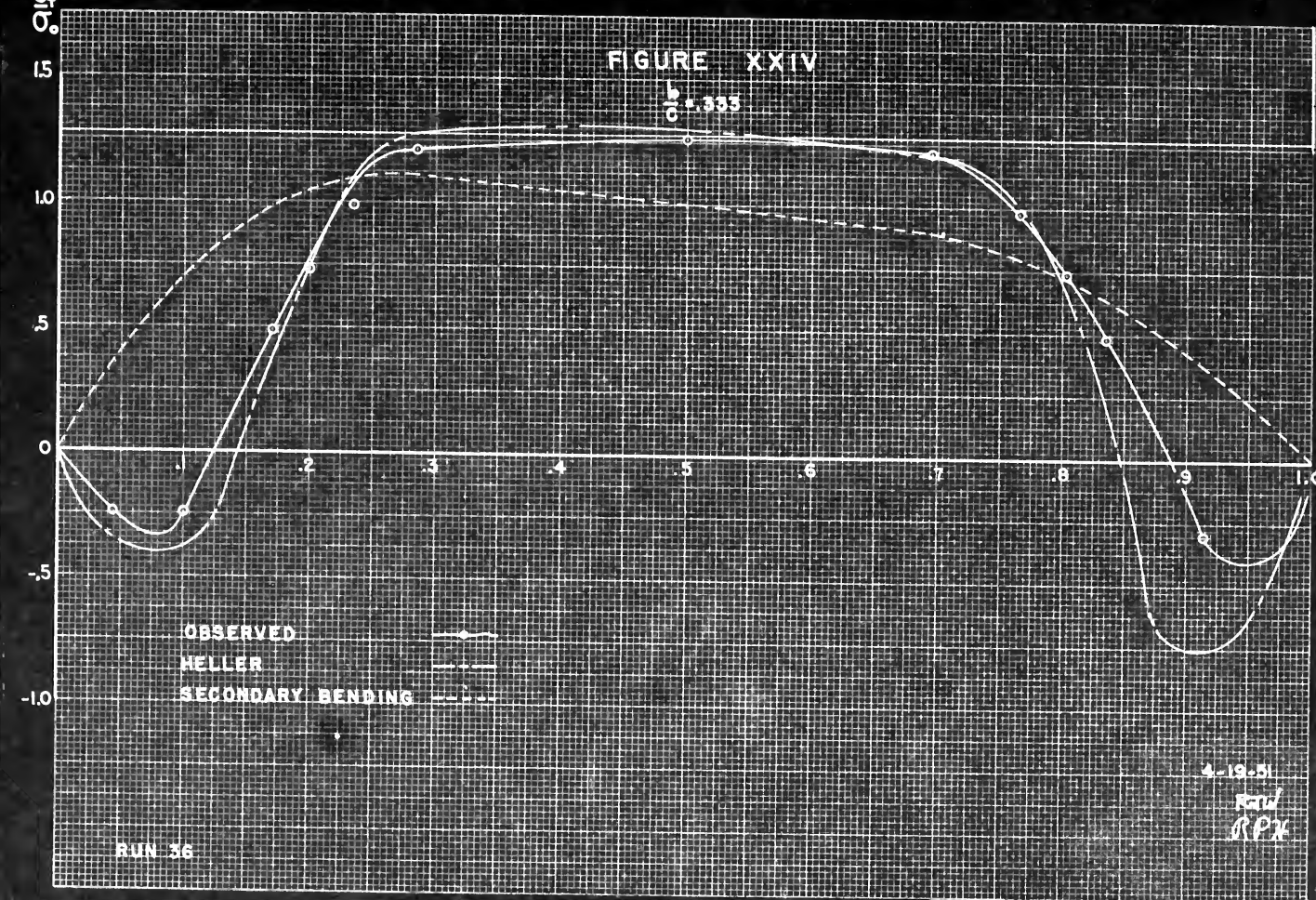
FIGURE XXIV
b/d = .333
1.5
1.0
.5
0
-.5
-1.0
.1
.2
.3
.4
.5
.6
.7
.8
.9
OBSERVED
HELLER
SECONDARY BENDING
RUN 36
4-19-51

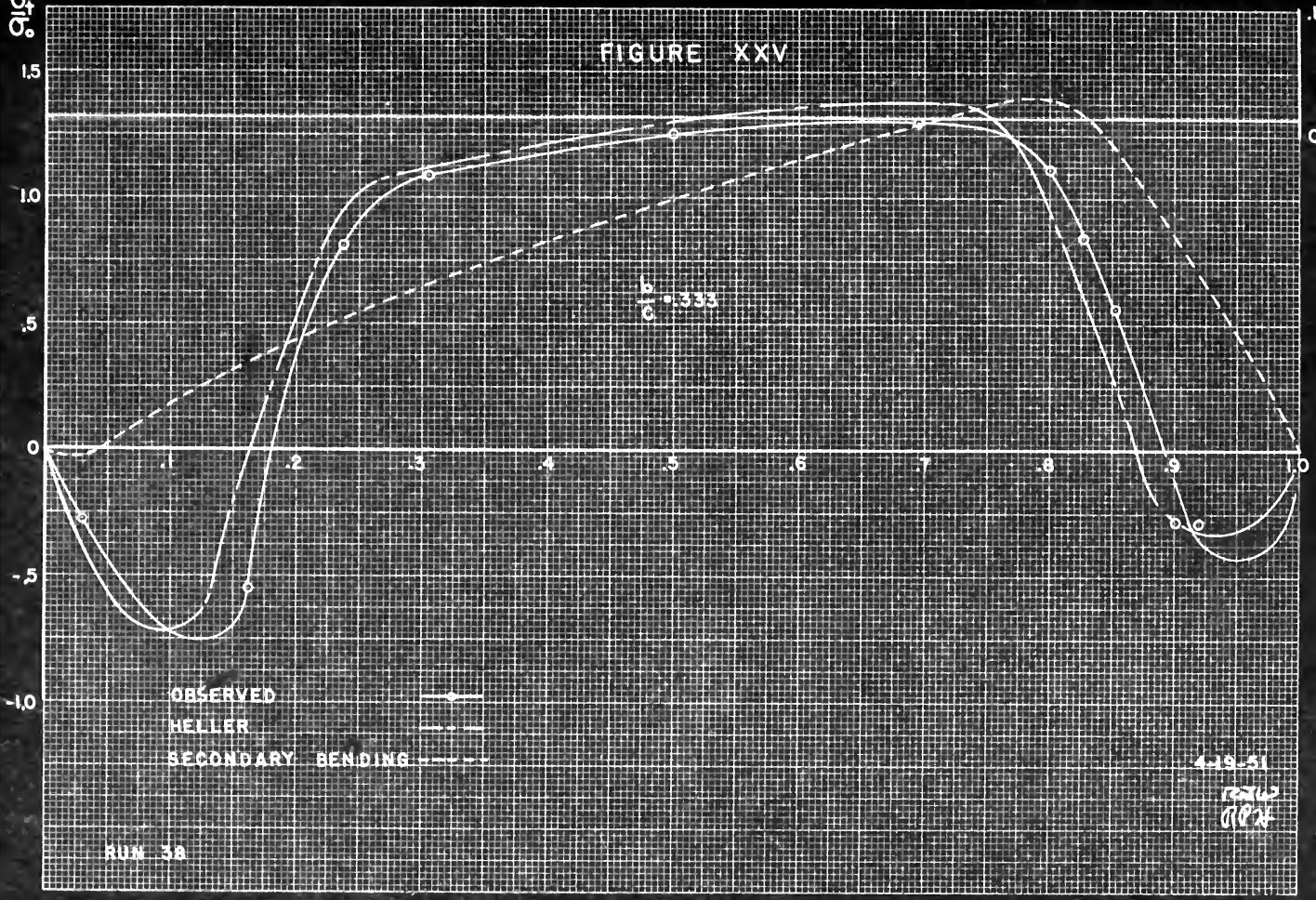
FIGURE XXV
1.5
1.0
.5
0
-.5
-1.0
.1
.2
.3
.4
.5
.6
.7
.8
.9
1.0
b/c = .333
OBSERVED
HELLER
SECONDARY BENDING
4-19-51
RUN 3A

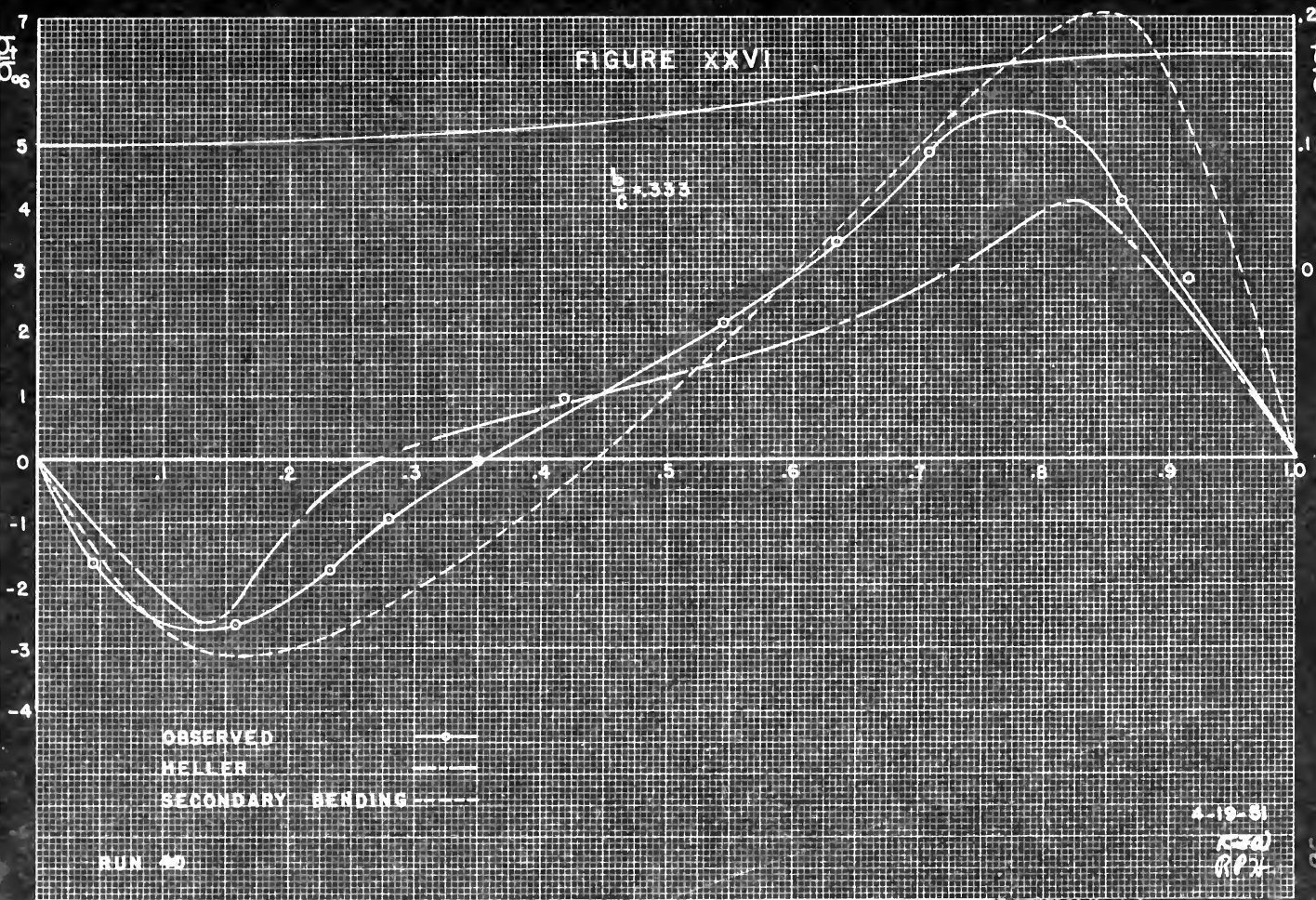
FIGURE XXVI
$\frac{b}{c}$ 6
5
4
3
2
1
0
-1
-2
-3
-4
.1
.2
.3
.4
.5
.6
.7
.8
.9
1.0
.2
.1
0
A-333
OBSERVED
WELLER
SECONDARY BENDING
RUN 40
4-19-51

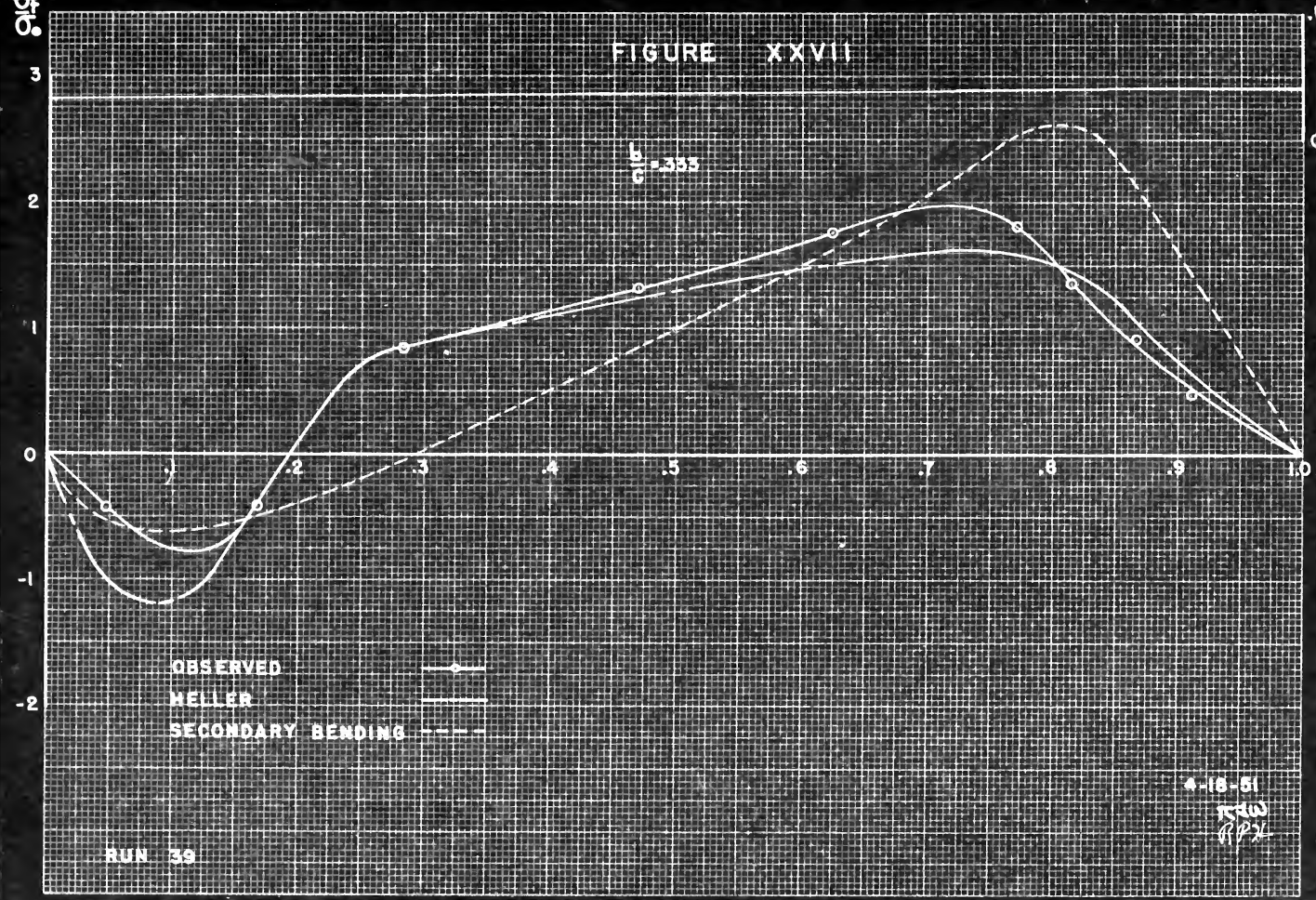
FIGURE XXVII
$\frac{b}{c}$=.333
3
2
1
0
-1
-2
.1
.2
.3
.4
.5
.6
.7
.8
.9
1.0
OBSERVED
HELLER
SECONDARY BENDING
RUN 39
4-18-51

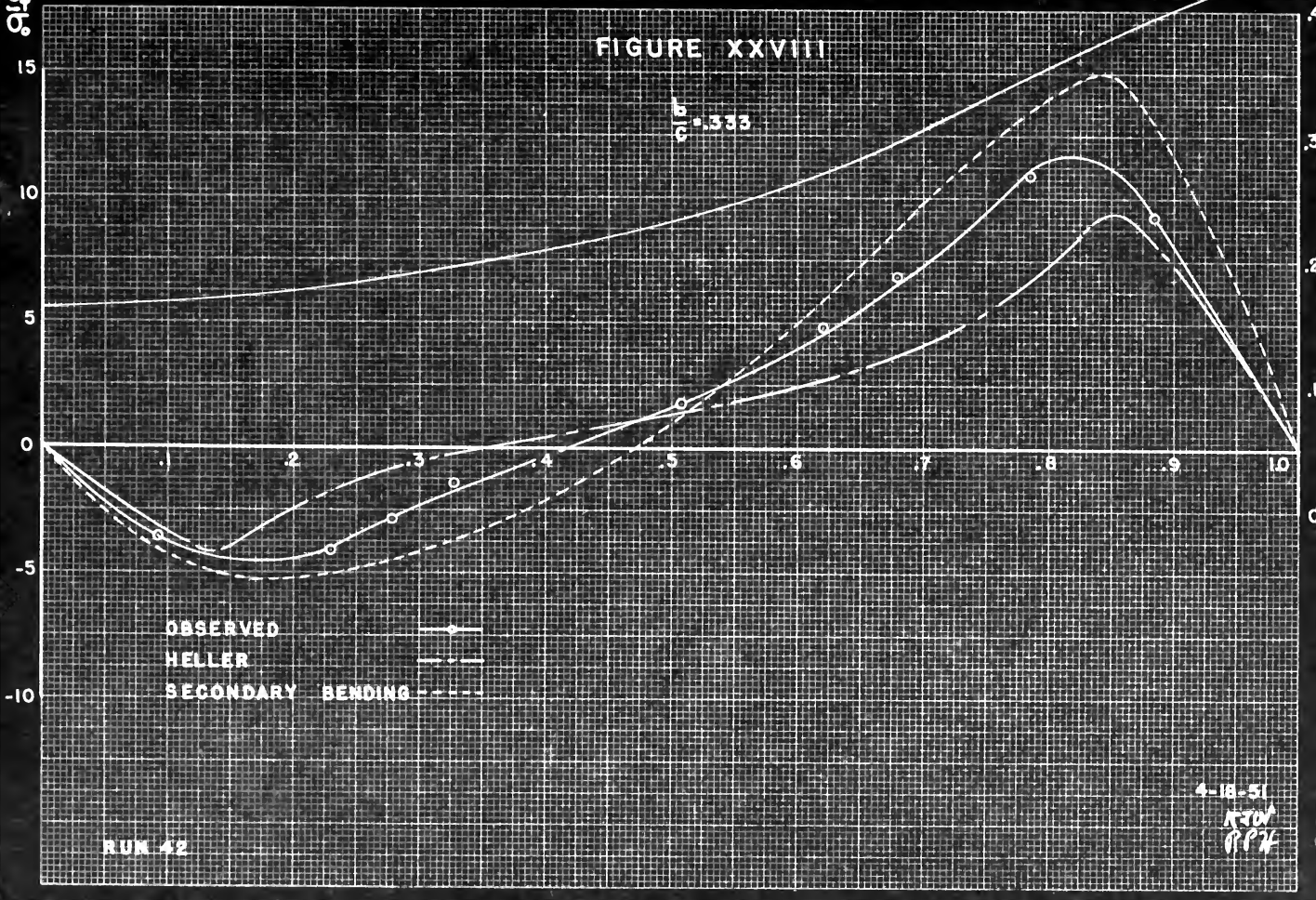
FIGURE XXVIII
b/c = .333
15
10
5
0
-5
-10
.1
.2
.3
.4
.5
.6
.7
.8
.9
1.0
OBSERVED
HELLER
SECONDARY BENDING
RUN 42
4-18-51

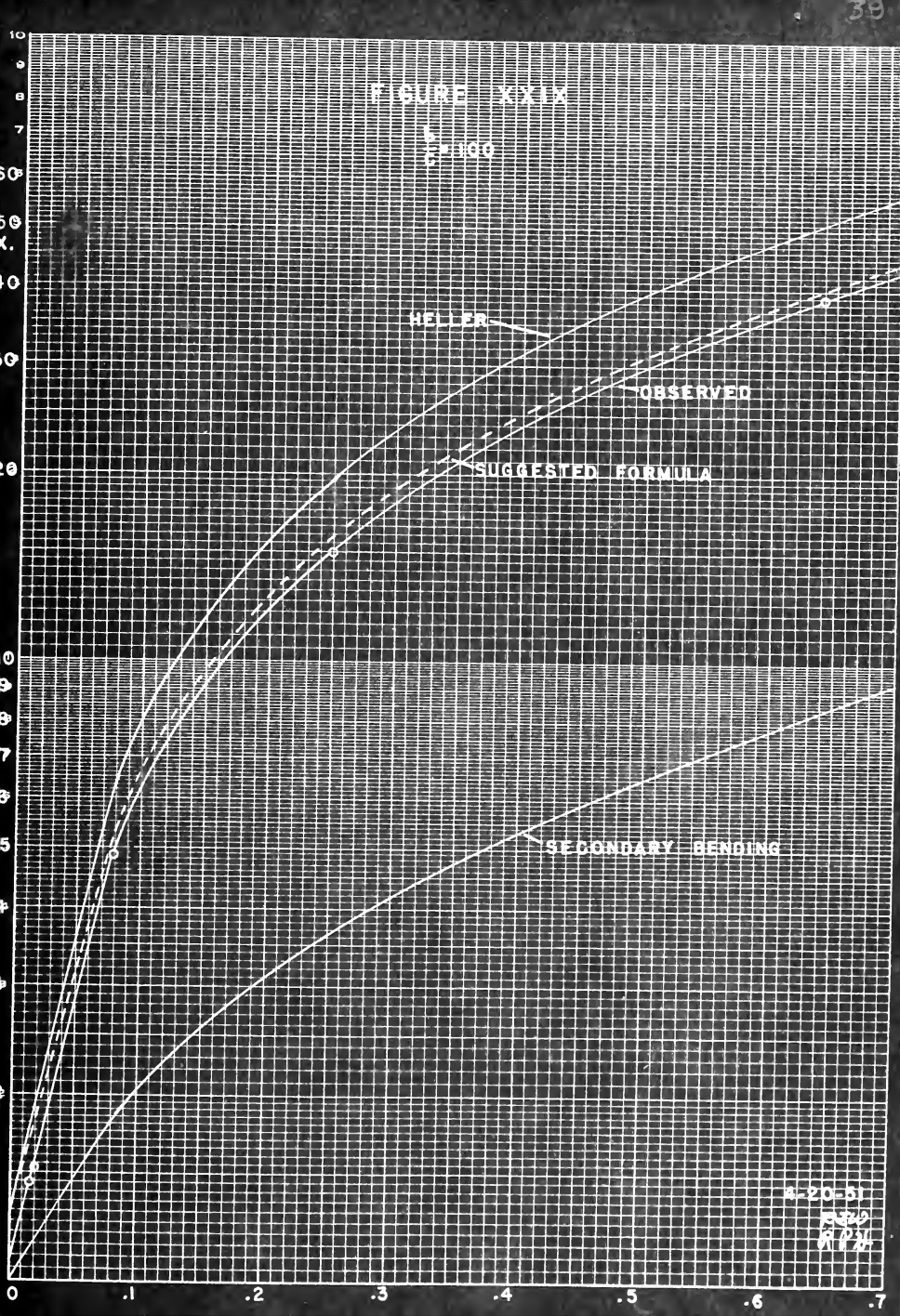
FIGURE XXIX
S/E=100
HELLER
OBSERVED
SUGGESTED FORMULA
SECONDARY BENDING
8-20-51
0
.1
.2
.3
.4
.5
.6
.7

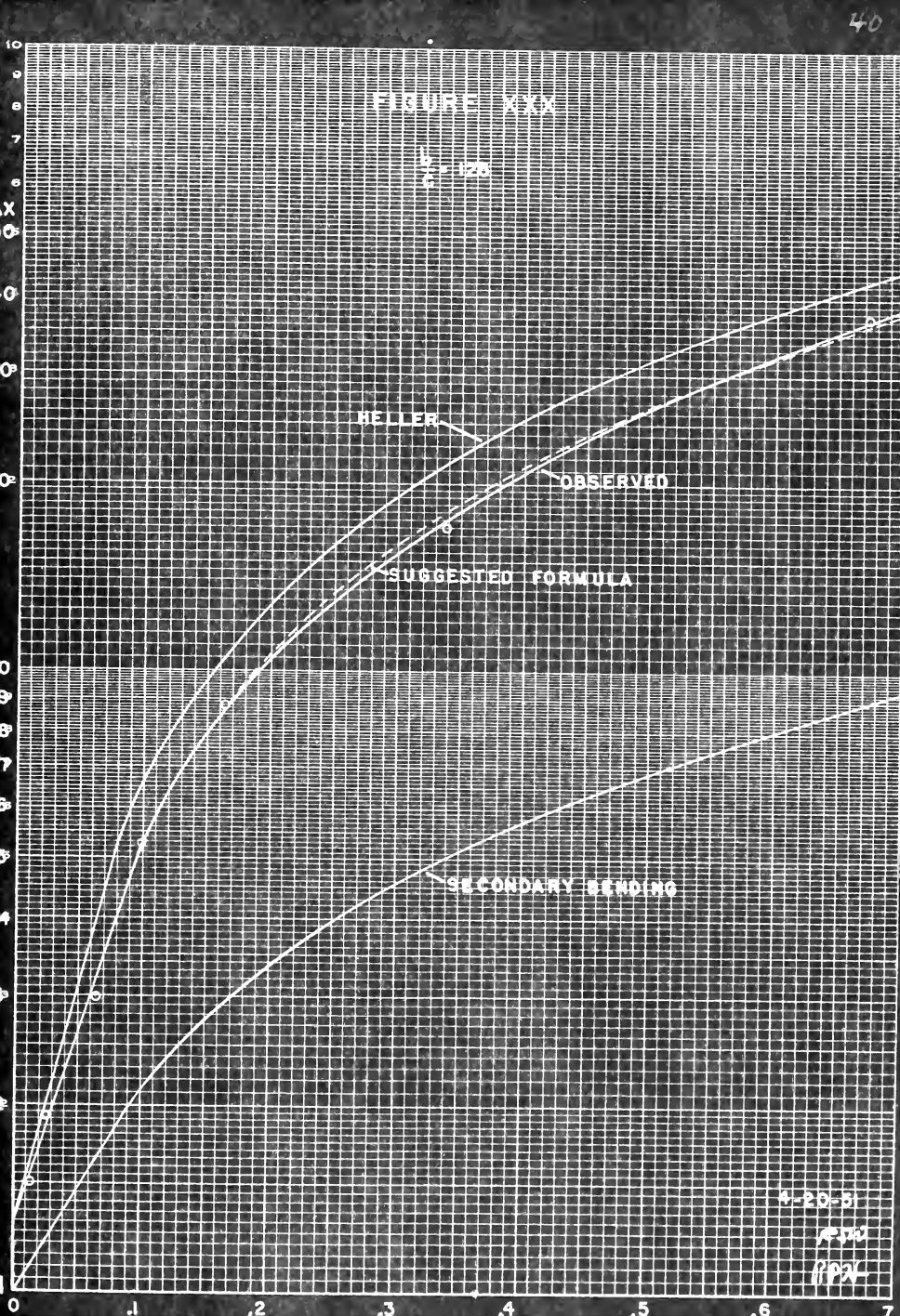
FIGURE XXX
HELLER
OBSERVED
SUGGESTED FORMULA
SECONDARY BENDING
4-20-31

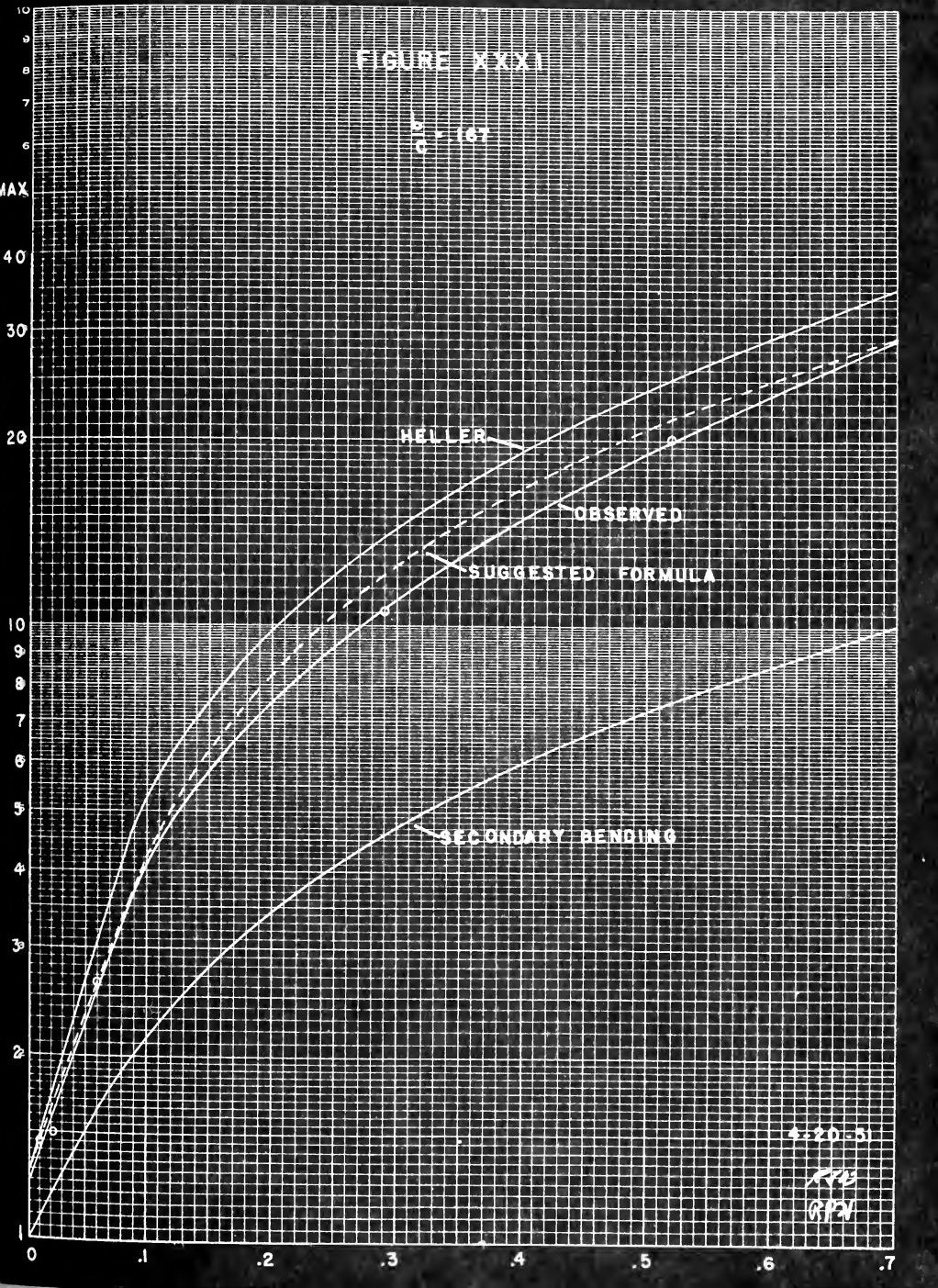
FIGURE XXXI
p/c = .167
MAX
HELLER
OBSERVED
SUGGESTED FORMULA
SECONDARY BENDING
4-20-53
0
.1
.2
.3
.4
.5
.6
.7

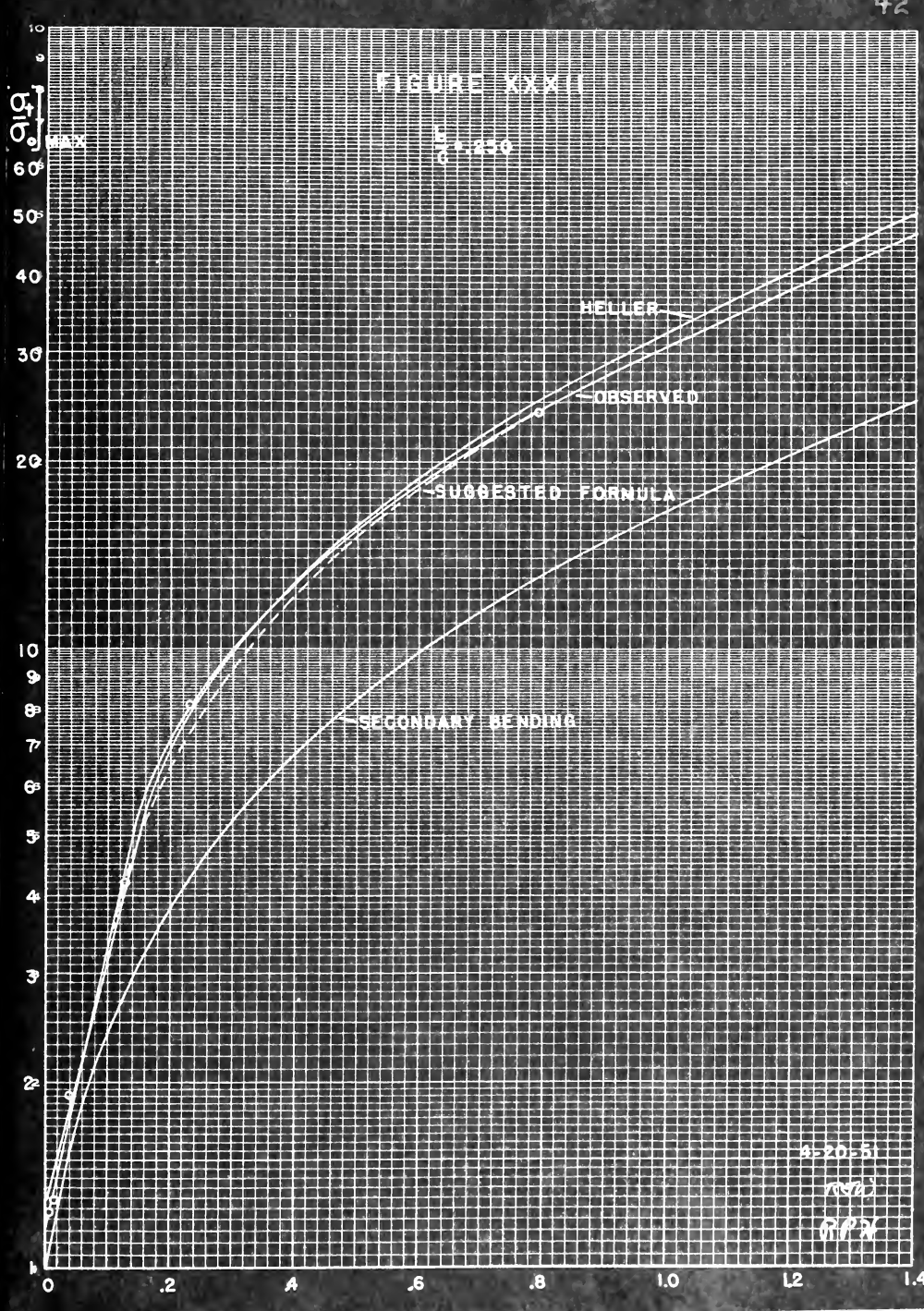
FIGURE XXXII
HELLER
OBSERVED
SUGGESTED FORMULA
SECONDARY BENDING
0
.2
.4
.6
.8
1.0
1.2
1.4

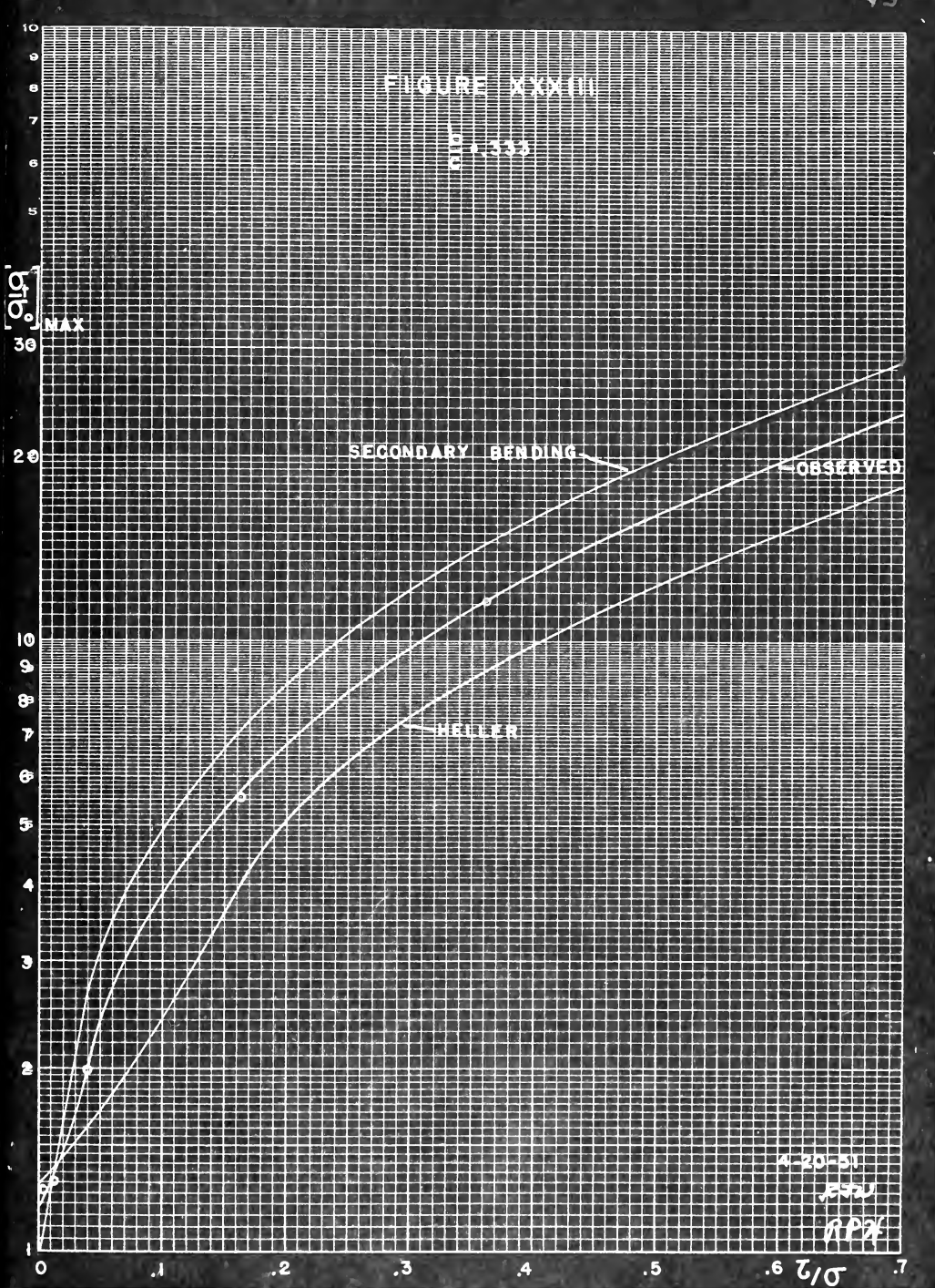
FIGURE XXXIII
$\frac{b}{a} = 1.333$
$\frac{\sigma_{max}}{\sigma}$
SECONDARY BENDING
OBSERVED
HEILER
A-20-50
JESSOP
RPK
$\sigma/2$
0
.1
.2
.3
.4
.5
.6
.7

DISCUSSION OF RESULTS

Heller's predicted stress at the boundary of an ovaloid of aspect ratio 2.0 agress remarkably well with the observed stress for ratios of hole-web depth from .100 to .333 and ratios of shear to bending stress ranging from zero to about 1.0. Hence, it is indicated that Heller's stated maximum limit of b/c of .20 is conservative.

For hole-web depth ratios less than about .250 the Heller maximum stress is greater than the observed maximum - and conversely for ratios greater than .250. The position of maximum stress shifts from the center of the hole (.500) towards the ends - approaching approximately .850 for shear to bending stress ratios greater than about .15; agreement between observed and predicted position is very good.

The secondary bending theory predicts stresses generally far less than the observed for hole-web depth ratios less than about .30. Fairly good agreement is noted for a hole-web depth ratio of .333. It is indicated that this theory will give maximum stresses in excess of the observed for hole-web depth ratios greater than about .30 and, if applied to structural desigh, will incorporate rather large inherent factors of safety. It is further indicated that the overall stress pattern about the hole is still best described by the Heller analysis.

Curves of observed maximum stress at various values of shear to bending stress ratios are easily derived noting that the function is essentially linear for values of greater than about .10 and exponential for ratios less than about .10. Noting the relatively large disagreement between the observed stress and the curve described by the simplified expression for this stress for b/c = .167 and the relation between the curves of observed stress for other values of hole-web ratio, suggests that the observed values of stress for b/c = .167 are a little low.

Any sources of inaccuracy in the experimental determination of the stress distribution at the hole boundary may be summarized as follows:

1. The presence of a dark ring visible in certain isochromatic photographs will tend to obscure the actual position of fringe intersections with the boundary and to alter the accuracy of the extrapolated fringe values at the boundary.
2. Machining limitations will affect ovaloid aspect ratio, boundary imperfections and eccentricity (in relation to web edges).
3. Any lack of symmetry in the residual stress and the hole boundary will result in inaccurate fringe order determinations.

4. Any variation from the measured weights of loading or dimensions between loads and hole; also, any eccentric application of loading.

CONCLUSIONS

1. Heller's solution for the stress at the boundary of an ovaloid of aspect ratio 2.0 in a web submitted to combined bending and shear is in good agreement with the observed values for hole-web depth ratios less than .250.

2. The secondary bending theory may be conservatively applied in structural design to those cases where the hole-depth ratio is greater than .333.

3. The maximum stress at the hole boundary for variable parameters of hole-web and shear-bending stress ratios is amenable to mathematical description.

RECOMMENDATIONS

1. Further experimental investigations for hole-web depth ratios greater than .333.

2. Investigation of the stress distribution at the web edges in way of the hole. This may be accomplished with the photographs of isochromatics included in Appendix E of this thesis. Results could be compared with secondary bending theory predictions.

3. Further experimental investigations of ovaloids of other than aspect ratio 2.0 - particularly 1.5. A simplified expression or nomograph for maximum stress could be derived including all three variable parameters: hole-web depth ratios, shear-bending stress ratios, and aspect ratio.

APPENDIX

APPENDIX A

SUPPLEMENTARY INTRODUCTION

I

The Stresses Around a Small Opening in a Beam Subjected to Bending with Shear. (Heller's Analysis.)

II

Introduction to the Secondary Bending Theory.

THE STRESSES AROUND A SMALL OPENING IN A BEAM SUBJECTED TO BENDING WITH SHEAR

by

S. R. Heller, Jr.[1], Cambridge, Mass.

This paper contains an exact closed solution for the stress distribution around a small opening in the web of a beam subjected to bending with shear. The complex variable method of solution for plane stress problems (Muschelišvili) is used. It is applied to the case of a general ovaloid opening (Greenspan). Curves showing the tangential stresses around the boundary are given for several common openings found in engineering structures (Joseph and Brock). Maximum stress concentration factors obtained are compared with those for similar openings subjected to tension, shear, and pure bending, as well as for similar cases of simpler geometry. The effect of small eccentricities in location is included.

Nomenclature

The following nomenclature is used in this paper:

(x,y) = Cartesian co-ordinates

(α,β) = Orthogonal curvilinear co-ordinates in general, and ovaloid co-ordinates in particular

$z = x + iy$

$w = \alpha + i\beta$

$\zeta = e^{w}$

$\lambda = e^{i\beta}$

J = Stretch ratio

γ = Angle in z-plane between tangent to curve, β = constant, and x-axis

Γ = Unit circle

[1] Student Officer, U.S.N.T.S. – M.I.T.

s, t, r = Real parameters

Φ, Ψ = Potential functions of complex variable z

φ, ψ = Potential functions of complex variable ζ

F = Airy stress function

σ_x, σ_y = Normal stresses; x is normal to surface for which x = constant, etc.

$\sigma_\alpha, \sigma_\beta$

$\tau_{\alpha\beta}, \tau_{xy}$ = Shear stresses

A_n, B_n = Complex constants

a_n, b_n

P = Applied load

L = Distance of applied load from center of hole

y_o = Half-height of opening

$= s - t + r$

e = Eccentricity of center of opening

I = Moment of inertia of beam

Γ = Shear parameter:

A_f, A_t, A_w = Flange area (gross), total area, web area (gross) respectively

h = Half-height of beam

$-$ = Bar above, indicates complex conjugate

Introduction

The purpose of this paper is to obtain an exact solution for the stress distribution at the boundary and in the neighborhood of an ovaloid opening in the web of a beam subjected to bending with shear, Fig. 1.

The beam is considered to be very long in the x-direction (practically infinite) and large (compared to the height of the opening; i. e., $y_o < 0.2h$)[2] but of finite extent in the y- direction.

---

[2] Cf. Figs. 6 and 7, pp. 216-217, [5]

The center of the opening is on the neutral axis; but, this is no limitation. The effect of eccentricity can be obtaine by superposition of known solutions for uniform tension or compression [1] and pure bending [2] plus an additional effect of shear which is included in the appendix to the solution considered here. The opening treated is called an ovaloid, and may be made to represent closely several common openings which occur in engineering structures.[3]

The method of solution used is that known as the complex-variable method, associated with the name of N. I. Muschelišvili. For a detailed treatment, see Sokolnikoff [3]. For an outline of the application of the method see Joseph and Frock [2] or Morkovin [4].

The problem of bending with shear has been solved using Airy stress functions for the circle by Howland and Stevenson [5] and for the ellipse by Leuber [6].

General Ovaloid Opening in a Beam Subjected to Bending with Shear

From [2] the following relations are obtained:

$$\left.\begin{aligned}\Phi(z) &= \sum^{\kappa}{}' A_n z^n + \sum^{\infty}{}' a_n z^{-n} \\ \Psi(z) &= \sum^{\kappa}{}' B_n z^n + \sum^{\infty}{}' b_n z^{-n}\end{aligned}\right\} \qquad (1)$$

$$\left.\begin{aligned}\sigma_x + \sigma_y &= 2\left[\Phi'(z) + \bar{\Phi}'(\bar{z})\right] = 4\,\mathrm{RE}\left[\Phi'(z)\right] \\ \sigma_y - \sigma_x + 2i\tau_{xy} &= 2\left[\bar{z}\,\Phi''(z) + \Psi'(z)\right] \\ F(x,y) &= \mathrm{RE}\left[\bar{z}\,\Phi(z) + \int \Psi(z)dz\right]\end{aligned}\right\} \qquad (2)$$

$$\left.\begin{aligned}\sigma_x + \sigma_y &= \sigma_\alpha + \sigma_\beta \\ \sigma_y - \sigma_x + 2i\tau_{xy} &= (\sigma_\beta - \sigma_\alpha + 2i\tau_{\alpha\beta})e^{-2i\chi}\end{aligned}\right\} \qquad (3)$$

From [3] and [4], the boundary equation for a free boundary

---

[3] The numbers in brackets refer to references in Bibliography.

is obtained:

$$\varphi(\lambda) + \frac{z(\lambda)}{z'(1/\lambda)} \cdot \overline{\varphi}'(1/\lambda) + \overline{\psi}(1/\lambda) = 0 \qquad (4)$$

From [1] and [4] the mapping function for the general ovaloid is obtained:

$$z = s\zeta + \frac{t}{\zeta} + \frac{r}{\zeta^3} \qquad (5)$$

Then, as is shown in [2] :

$$J_o^2 = s^2 + t^2 + 9r^2 - 2t(s - 3r)\cos 2\beta - 6rs \cos 4\beta \qquad (6)$$

At distances remote from the opening ($|x|>4h$), the stress distribution corresponding to Fig. 1 is:

$$\sigma_x = \frac{P(L - x)y}{I} \; ; \quad \sigma_y = 0 \; ; \quad \tau_{xy} = -\tau\Gamma + \frac{Py^2}{2I} \qquad (7)$$

where: $\tau = \frac{P}{2ht_w} = \frac{P}{A_w}$

$$\Gamma = \frac{3}{(1 - \frac{t_f}{h})} - \frac{h^2 A_w}{I} \cdot \frac{A_f/A_t}{1 - A_f/A_t}$$ [4]

t_f, t_w = Flange thickness, web thickness respectively

The boundary conditions, Equations (7), are equivalent to a "Pure Bending" Component: $\sigma_x = \frac{Ply}{I}$; $\sigma_y = 0$; $\tau_{xy} = 0$ (7a)

and "Bending with Shear": $\sigma_x = -\frac{Pxy}{I}$; $\sigma_y = 0$; $\tau_{xy} = -\tau\Gamma + \frac{Py^2}{2I}$ (7b)

The solution for pure bending [2] will be used later. For the present, the solution for boundary condition, Equation (7b), will be sought.

The substitution of Equations (1) and (7b) into the first two of Equations (2), for large values of x, yields:

$$A_3 = \frac{iP}{2I} \; ; \quad B_1 = -i\tau\Gamma \; ; \quad B_3 = -\frac{iP}{12I} \qquad (8)$$

---

[4] This is based on approximate theory that the web of an I-beam takes most of the shearing force and that the shearing stresses are constant across the web thickness. Cf. p305, [7].

which are valid for any opening regardless of shape.

When Equations (1) with values from Equations (.) and Equations (2) as modified by the co-ordinate transformation equations (3) and the mapping function (5) are substituted in the boundary equation (4), it becomes:

$$\varphi(\lambda) - (s\lambda + \frac{t}{\lambda} + \frac{r}{\lambda^3}) \left[\frac{iP}{\pi I}(\frac{s}{\lambda} + t\lambda + r\lambda^3)^2 + \sum_1^\infty \frac{n\bar{a}_n}{(\frac{s}{\lambda} + t\lambda + r\lambda^3)^{n+1}} \right] +$$

$$+ i\tau\Gamma(\frac{s}{\lambda} + t\lambda + r\lambda^3) + \frac{iP}{\pi I}(\frac{s}{\lambda} + t\lambda + r\lambda^3)^3 + \sum_1^\infty \frac{\bar{b}_n}{(\frac{s}{\lambda} + t\lambda + r\lambda^3)^n} = 0 \quad (9)$$

Multiplying by $\frac{d\lambda}{2\pi i(\lambda - \zeta)}$, integrating around γ with the aid of the Cauchy Integral Theorems, we get:

$$-\varphi(\zeta) + \frac{iP}{2\pi I}(s^3\zeta^3 + 3s^2t\zeta) + \frac{iP}{\pi I} \cdot \frac{rs^2}{\zeta^3} + \frac{iP}{4\pi I} \cdot \frac{(6rst + 3s^2t - 2s^3)}{\zeta^3} +$$

$$+ \frac{iP}{8\pi I} \cdot \frac{(s^3 + 2st^2 + rt^2 + 2sr^2 - 2s^2t - 8\tau\Gamma Is/P)}{\zeta} + \frac{r\bar{a}_1}{\zeta s^2} = 0 \quad (10)$$

Multiplying by $\frac{\lambda d\lambda}{2\pi i(\lambda - \zeta)}$ and integrating around γ, we get:

$$-\zeta\varphi(\zeta) + \frac{iP}{2\pi I} \cdot (s^3\zeta^4 + 3s^2t\zeta^2 + 3s^2r + 3st^2) + \frac{iP}{8\pi I} \cdot \frac{rs^2}{\zeta^4} +$$

$$+ \frac{iP}{24\pi I} \cdot \frac{(6rst + 3s^2t - 2s^3)}{\zeta^2} + \frac{a_1}{s} = 0 \quad (11)$$

From Equations (10) and (11):

$$a_1 = \frac{iPs^2}{\pi I} \cdot \frac{(s^3 + st^2 + rt^2 + 2sr^2 - 2s^2t - s^2r - 8\tau\Gamma Is/P)}{(r + s)} \quad (12)$$

and

$$\varphi(\zeta) = \frac{iPs}{2\pi I}\left[s^2\zeta^3 + 3st\zeta + \frac{3(s^3 - 2s^2t + 3sr^2 + 2st^2 + 2rt^2 - 8\tau\Gamma Is/P)}{(r + s)\zeta} + \right.$$

$$\left. + \frac{6rt + 3st - 2s^2}{\zeta^3} + \frac{3rs}{\zeta^5}\right] \quad (13)$$

The substitution of Equation (13) into the first of Equations (2) as modified by Equations (3) and the first of Equations (3) yields:

$$(\sigma_\beta)'_{\alpha=0} = -\frac{Ps}{2IJ_0^2}\left\{\left[s^3 + 2s^2t - 4st^2 - 15sr^2 - 6rt^2 + \right.\right.$$

$$+ \frac{s+3r}{s+r}(s^3 - 2s^2t + 2st^2 + 3sr^2 + 2rt^2 - 8\tau\Gamma Is/P)\left.\right]\sin 2\beta -$$

$$\left. - 2s(s^2 - st + rt)\sin 4\beta + 2s^2r \sin 6\beta\right\} \qquad (14)$$

Repeating the process which led to Equation (13) by using the conjugate of Equation (4), we get:

$$\psi(\zeta) = \frac{iPs}{24I}\left[\frac{s^2}{\zeta^3} + \frac{3st}{\zeta} + 3A\zeta + 3\zeta^3 + 3rs\zeta^5 - \right.$$

$$\left. - \frac{s + t\zeta^2 + r\zeta^4}{s\zeta^4 - t\zeta^2 - 3r}(3s^2\zeta^5 + 3st - 3A\zeta - \frac{3B}{\zeta} - \frac{15rs}{\zeta^3})\right] \qquad (15)$$

where: $A = \frac{s^3 - 2s^2t + 3sr^2 + 2st^2 + 2rt^2 - 8\tau\Gamma Is/P}{r+s}$

and $B = 6rt + 3st - 2s^2$

The insertion of Equations (13) and (15) into the last of Equations (2) gives:

$$F(\alpha, \beta) = \frac{Ps^2}{24I}\left[g_1(\alpha)\sin 2\beta + g_2(\alpha)\sin 4\beta + g_3(\alpha)\sin 6\beta\right]$$

where: $g_1(\alpha) = -s^2e^{-4\alpha} + \frac{e^{-4\alpha}}{2}(3s^2 + 3t^2 - 3A + 9r^2 + \frac{2t}{s} - \frac{3Ar}{s}) +$

$$+ 3(A - t^2) + \frac{e^{-2\alpha}}{3}(-s^2 + 3t^2 - 3A - 15r^2 + \frac{9Ar}{s} - \frac{3Bt}{s}) +$$

$$+ e^{-4\alpha}(\frac{3t}{s} - \frac{3Ar}{s}) + 3r^2e^{-8\alpha}$$

$$g_2(\alpha) = \frac{e^{4\alpha}}{4}(3st + 6rt - B) - ste^{2\alpha} + e^{-2\alpha}(B - 3rt) +$$

$$+ \frac{e^{-4\alpha}}{4}(st - 6rt - 3B) + 3rte^{-6\alpha}$$

$$g_3(\alpha) = -rs(1 - 3e^{-4\alpha} + 2e^{-6\alpha}) \qquad (16)$$

Equations (14) and (16) agree with [5] for the circle ($r = t = 0$) and with [6] for the ellipse ($r = 0$) for the rectangular strip ($\Gamma = 1.5$).

We now define an additional criterion, the shear stress to bending stress ratio, $(\frac{\tau}{\sigma})$, wherein:

τ is the average shear stress at the location of the opening if there were no opening;

σ is the nominal bending stress at the extreme fibers at the location of the opening, if there were no opening.

Thus: $\tau = \frac{P}{2ht_w}$ and $\sigma = \frac{PLh}{I}$

And: $$\frac{\tau}{\sigma} = \frac{I}{2h^2 t_w L} \qquad (17)$$

We take as reference stress the nominal bending stress at the edge of the opening if there were no opening:

$$\frac{PLy_o}{I}$$

Then, noting that L >> s, t, r, equation (14) becomes:

$$\frac{(\sigma_\beta)_{\alpha=0}}{\frac{PLy_o}{I}} = \frac{4s^2(s+3r)}{y_o^2(s+r)} \Gamma \cdot \frac{h}{y_o} \cdot \frac{\tau}{\sigma} \sin 2\beta \qquad (14a)$$

We now superpose equation (14a) on equation (27) of [2] which gives the stress distribution for the condition of Fig. 1:

$$\frac{(\sigma_\beta)_{\alpha=0}}{\frac{PLy_o}{I}} = \frac{s}{y_o^2 \delta} \Big[(s^2 + 3rt + \frac{3r^2 t}{s} - 3rs - 2t^2 - \frac{2rt^2}{s} + st - 12r^2)\sin\beta +$$

$$+ \frac{4sy_o(s+3r)}{s+r} \Gamma \frac{h}{y_o} \frac{\tau}{\sigma} \sin 3\beta - (rt - st + s^2)\sin 3\beta +$$

$$+ rs \sin 5\beta \Big] \qquad \text{for } 0 < \frac{y_o}{h} < 0.4 \qquad (14)$$

Equation (14) gives the effect of shear. If we do not take as reference stress, the average shear stress, Equation (14) now becomes:

$$\frac{(\sigma_\beta)_{\alpha=0}}{\frac{P}{2ht_w}} = -\frac{s^2 h t_w}{I y_o} \Big\{ \Big[s^2 + 3st - 4t^2 - 15r^2 - \frac{6rt^2}{s} + \frac{(s+3r)}{s+r}(s^2 -$$

$$- 3st + s^2 + 3r^2 + \frac{3rt^2}{s} - 3\tau\Gamma I/P) \Big] \sin 2\beta -$$

$$- 2(s^2 - st + rt)\sin 4\beta + 2rs \sin 6\beta \Big\} \qquad (14b)$$

$$\cong \frac{4s^2 \Gamma (s+3r)\sin 2\beta}{y_o^2 (s+r)}$$

For the usual values of s, t, and r (see Numerical Cases) the shear effect dominates equation (14) when $\frac{\tau}{\sigma} > 0.2$. In fact when

the shear stress - bending stress ratio exceeds 0.3 the point of maximum stress coincides with that given by Equation (14a):

$$12rs\cos^3 2\beta - (s^2 + t^2 + 9r^2 - 16rs)\cos 2\beta + (2st - 6rt) = 0 \quad (19)$$

The roots of Equation (19) may be extracted by means of a nomographic chart similar to Fig. 3, [ ] . Furthermore, with the exception of Case 4 ("Square" with diagonal vertical), the maximum stress so determined from Equation (14a) approaches that determined by Equation (18) asymptotically and at $\frac{\tau}{\sigma} = 0.3$ is in error by only 4%.

Numerical Cases

Following [1] and [2] , we obtain the tangential stresses, σ_t, along the inner boundary, $\alpha = 0$, for four simple cases, for $\Gamma = 1.5$.

Case 1 (Figs. 3 & 4). Cycloid hole, major axis horizontal, for which $s = 1.586$, $t = 0.471$, $r = -0.079$, $\frac{\xi_o}{R} = 0.1$.

$$\frac{\sigma_t}{\frac{PLy_o}{I}} = \frac{4.508 \sin\beta + 13.21 \tau/\sigma \sin 2\beta - 2.592 \sin 3\beta - 0.123 \sin 5\beta}{2.800 - 1.743 \cos 2\beta + 0.752 \cos 4\beta}$$

$$\frac{\sigma_t'}{\frac{P}{2ht_w}} = \frac{13.280 \sin 2\beta + 0.123 \sin 4\beta + 0.002 \sin 6\beta}{2.800 - 1.743 \cos 2\beta + 0.752 \cos 4\beta} \cong \frac{13.51 \sin 2\beta}{2.8 - 1.743 \cos 2\beta + 0.752 \cos 4\beta}$$

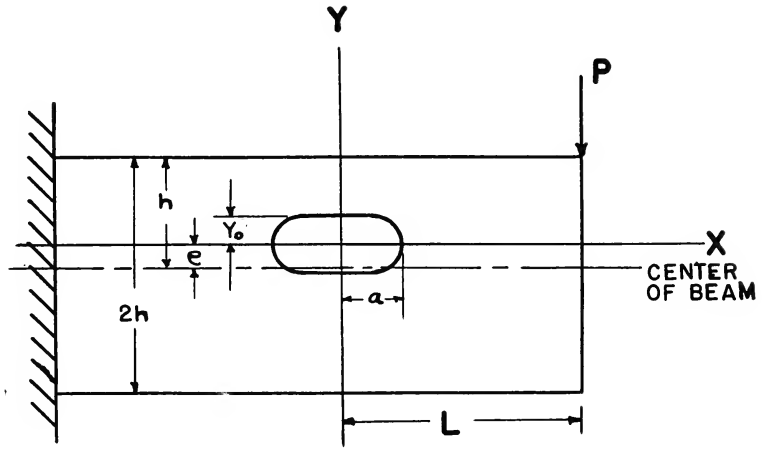

Fig. 1 Geometry and Notation of Beam Containing an Opening and Subjected to Bending With Shear.

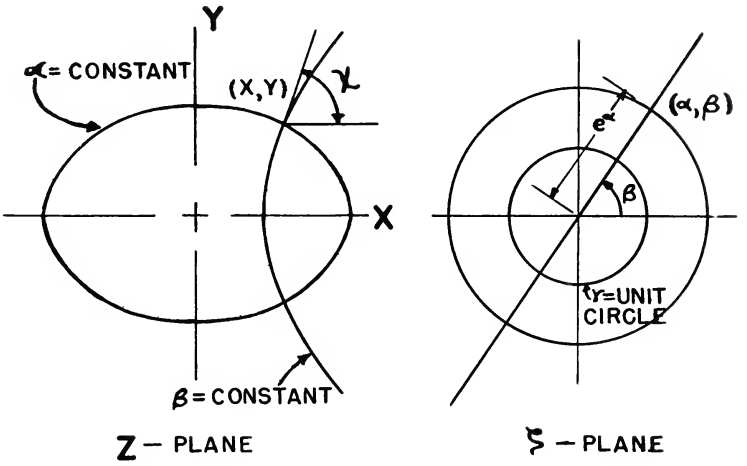

Fig. 2 Geometry and Notation for Transformation of Coordinates.

FIGURE 3

[illegible] OUTLET) HOLE, MINOR AXIS VERTICAL

(DISTRIBUTION ALONG BOUNDARY OF STRESS

DUE TO BENDING WITH SHEAR)

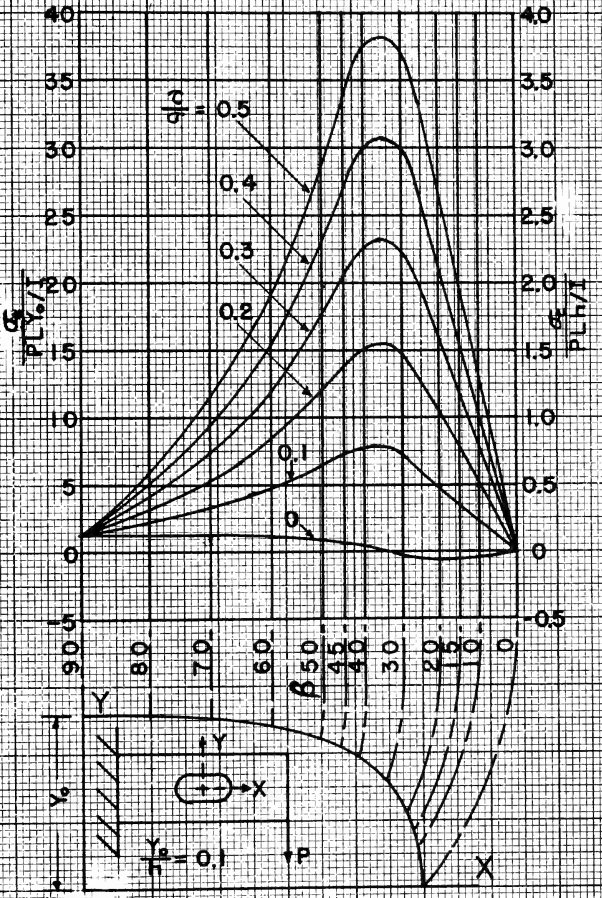

INTRODUCTION TO THE SECONDARY BENDING THEORY

The secondary bending theory is based on the concept that the portions of the web above and below the hole can be treated as cantilevers subjected to an end loading. The sum of the two end loadings is assumed equal to the total shear in the web. Assuming the same deflection at the ends of the two cantilevers, it is apparent that each loading is proportional to the moment of inertia of that cantilever - or, more simply, its depth cubed; thus for a hole symmetrical about the web's longitudinal axis, the loadings are equal and one-half of the total web shear. The secondary bending stress in the "cantilever" is determined by the usual bending stress formula. This stress is superposed upon the bending stress calculated by the same formula for the web without the hole at any given point. The theory may be expressed by the formulae given below. Nomenclature is indicated in the accompanying sketch.

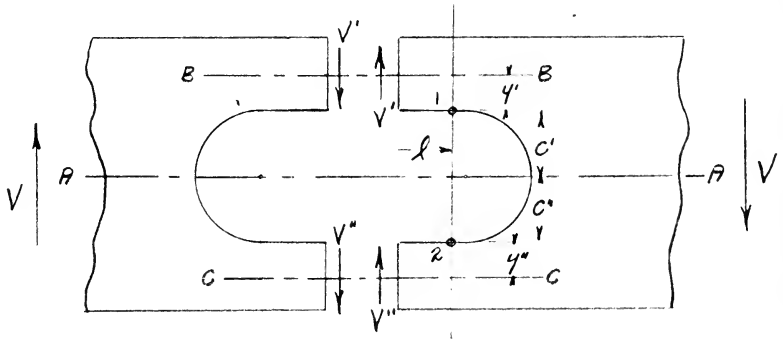

$$\sigma_1 = \frac{Mc'}{I_{AA}} + \frac{V'y'\ell}{I_{BB}} \qquad \sigma_2 = \frac{Mc''}{I_{AA}} + \frac{V''y''\ell}{I_{CC}}$$

$$\text{Where } V = V' + V'' \quad \& \quad \frac{V'}{V''} = \frac{I_{BB}}{I_{CC}}$$

APPENDIX B

DETAILS OF PROCEDURE

1. Details and dimensions of the model, tensile test specimen and test equipment are depicted in Figure XXXIV-A. Critical dimensions were machined in all cases to within .001".
2. Defender Process Ortho 4x5 film was submitted to about one-minute exposures in obtaining the photographs of model isochromatics. The use of this film permitted visual observation during developing - hence insuring optimum reproduction of fringes. Dupont #3 velour black glossy photographic paper was found to afford maximum fringe clarity upon printing.
3. The model was annealed in the Photoelasticity Laboratory annealing oven. An oil bath was used. Temperature was raised to 220°F. in approximately two and one-half hours and maintained constant for about the same length of time. Cooling to room temperature was accomplished in the closed oven in about 12 hours. The annealings were moderately effective in removing the small values of time-edge effect encountered. The model was immersed in an oil bath when not being subjected to machining or

experimentation in accordance with the theory that such procedure may decrease the polymerization of the material.

4. A 3/4" high-speed steel end mill was used for the machining of web edges on the material.

5. The initial step in the photoelastic analysis was to determine the residual stress in the model for each group of runs. It was possible to ascertain very accurately the value and sign of the residual stress at the hole if the hole were not there by simultaneous analysis of the no-load and pure bending photographs for each group of runs. This residual stress was in all cases tensile and less than 0.4 fringe order. However, it was impossible to accurately determine the net value of the residual stress at the hole boundary after machining stresses and time-edge effect had been superposed on this tensile field.

But two salient facts permit a detour about this obstacle:

(a) The no-load photographs indicate that the resultant residual stresses at the hole boundary are very nearly symmetrical about the horizontal axis.

(b) Stress theory and symmetry suggest that the

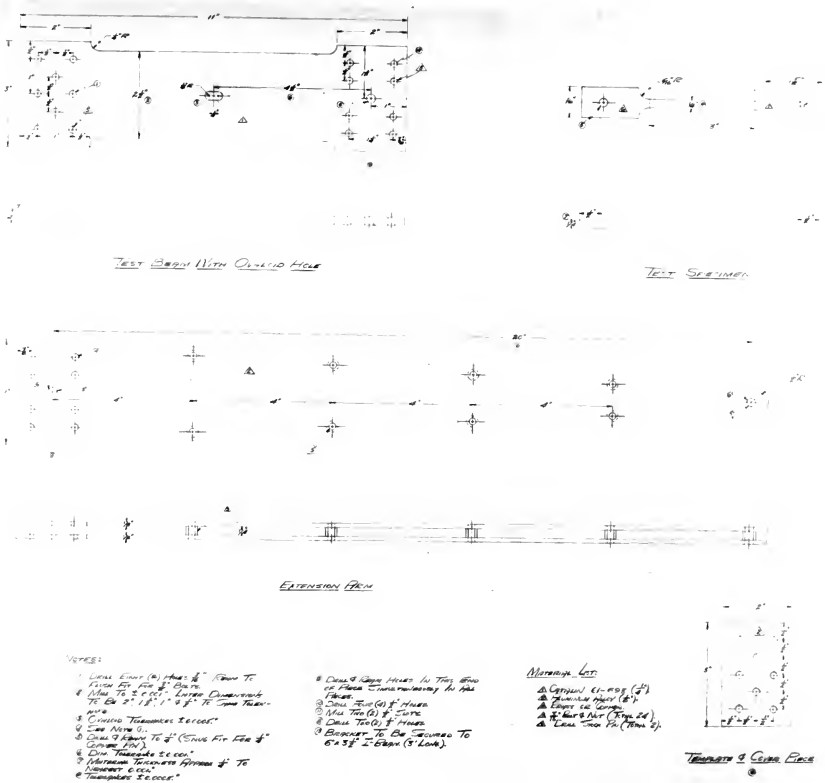

FIGURE XXXIV-A

TESTING EQUIPMENT DETAILS

hole boundary stresses should be of the same magnitude (but different sign) at vertically opposite points.

Hence, resort to a rather commonly used tool of the photoelastic analyst is justified here; namely, at any arbitrary vertical station the two values of fringe order may be averaged to obtain a value very close to the true value. This procedure was followed throughout.

A minimum of nine stations was used for each photograph. By symmetry and bending stress theory it is obvious that the two end stations must have a value of zero. Four stations, at least, were selected in the expected vicinity of the two peak values of stress concentration; these regions were either obvious from examination of the photograph or were closely predicted by the two theoretical solutions treated in this paper. Fringe values uncorrected for residual stress were obtained either at intersections of isochromatics with the hole boundary or by extrapolation to the hole boundary of a curve of fringe order versus fringe position.

The corrected value of the fringe order at the hole boundary is a measure of the tangential stress at that boundary since the isochromatic is, by defi-

nition, the locus of points representative of constant principal stress difference, and the principal stress normal to the free boundary at the boundary is zero.

APPENDIX C

SUMMARY OF DATA AND CALCULATIONS

1. Photoelastic analysis:

   (a) Table II presents loadings and resultant shear and moments subjected on the model at the various web depths.

   (b) Variation in moment across the hole was taken into account.

   (c) The value of the stress at a distance "b" from the neutral axis (σ_o) was computed from the primary bending stress formula. Application of the material fringe constant allowed conversion of this stress value to fringe order.

   (d) The results of the tensile test specimen runs to determine the fringe constant are presented in Fig. XXXIV-B.

2. Heller's Analysis:

   (a) The values of r, s, and t used in Case I of Heller's paper are for a curve closely approximating an ovaloid of aspect ratio 2.0 and, hence, are used in his equation 31b.*

   (b) Moment variation across the hole was taken into account.

---

* See pp.51-56, Ref.(6).

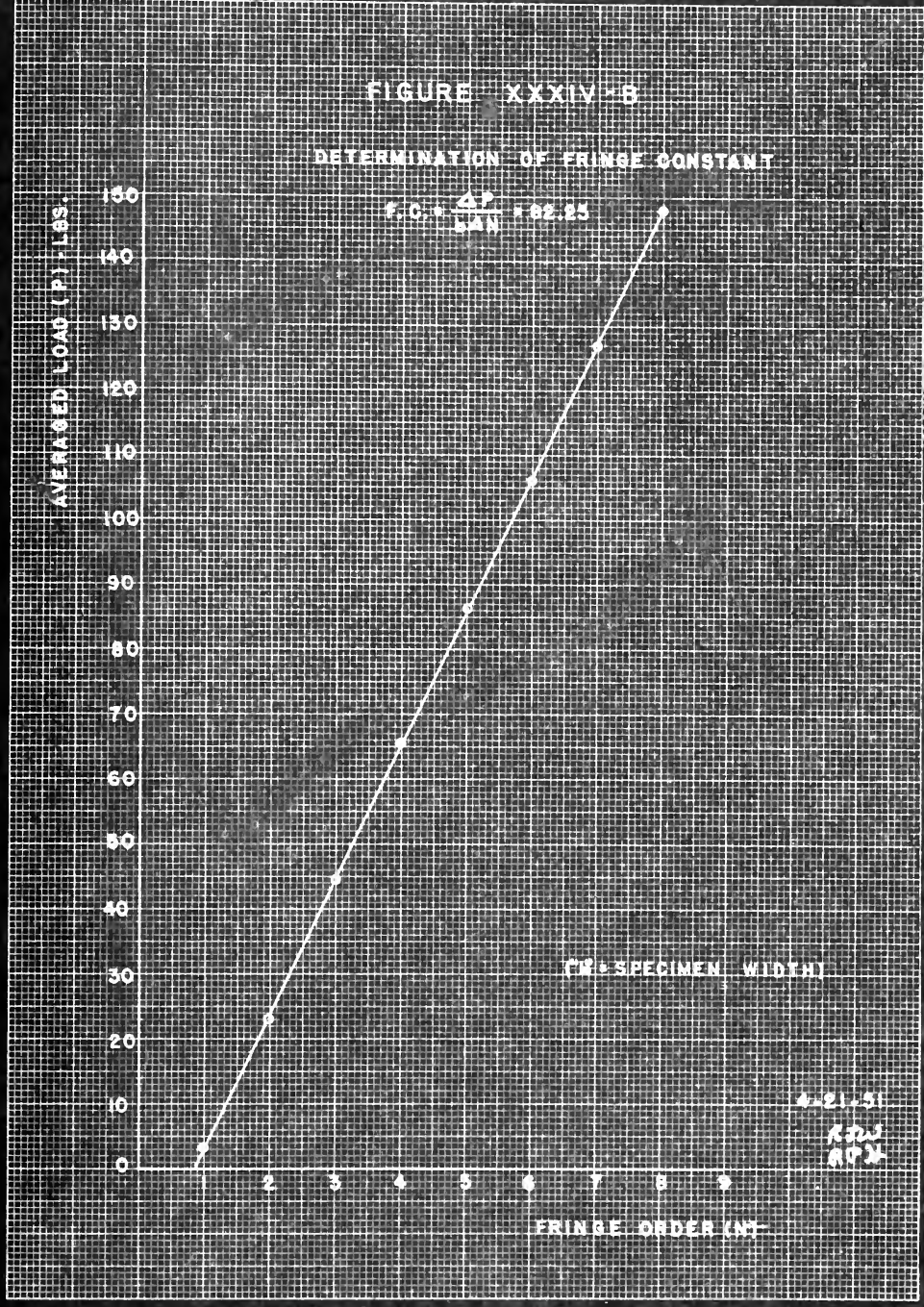
FIGURE XXXIV-B
DETERMINATION OF FRINGE CONSTANT
F.C. = 4F/BAN = 82.25
(APPLIED LOAD (P) - LBS.)
150
140
130
120
110
100
90
80
70
60
50
40
30
20
10
0
1
2
3
4
5
6
7
8
9
(B = SPECIMEN WIDTH)
A = 21.51
FRINGE ORDER (N)

(c) The equation had to be modified for most of the runs, as indicated in the Sample Calculations.

3. Secondary bending analysis:

(a) The curves of stress distribution predicted by secondary bending theory were extrapolated to zero at the hole ends - although the form of the curve is questionable. It is obvious that application of this theory to both upper and lower boundaries of the ovaloid will result in a net stress of zero at the neutral axis - but it is not possible to ascertain where the influence of one boundary application affects the other.

TABLE I

NOMENCLATURE

$2a$	-	Ovaloid major axis
$2b$	-	Ovaloid minor axis
β	-	Ovaloid eccentric angle (Heller's analysis)
$2c$	-	Web depth
I	-	Web moment of inertia = $\frac{2c^3t}{3}$
M	-	Bending moment
P	-	Applied loads
σ	-	Bending stress at web edge without ovaloid = $\frac{Mc}{I}$
σ_o	-	Bending stress at distance "b" from web neutral axis without ovaloid = $\frac{Mb}{I}$
σ_t	-	Tangential stress at ovaloid boundary
t	-	Web thickness
τ	-	Average shear stress = $\frac{V}{2ct}$
V	-	Shear force
Sta.	-	Ovaloid boundary position (abscissae Figs. II-XXVIII)

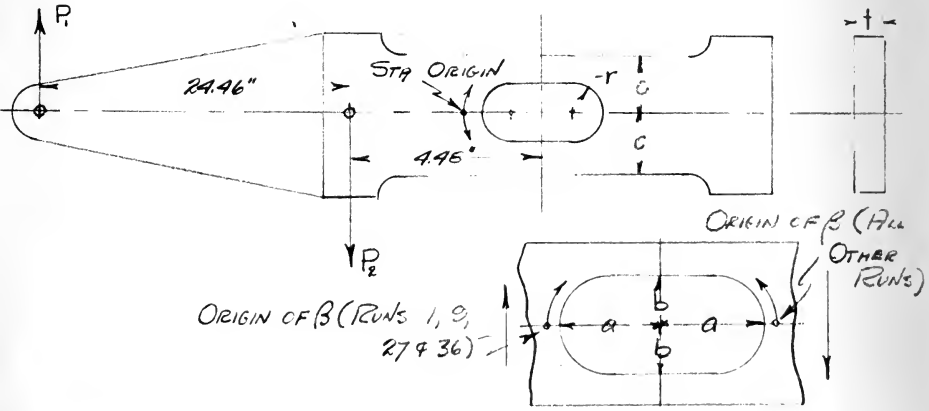

TABLE II

RUN	P_1 (#)	P_2 (#)	M_o (11-")	V (#)	$\frac{V}{M_o}$	C (")	$\frac{b}{c}$
0				NO LOAD		2.50	.100
1	42.69	0	1025	40.94	.0400		
3	42.69	75.44	686	35.50	.0517		
4	42.15	123.25	460	82.85	.180		
5	31.88	128.25	185	98.13	.531		
6	27.88	128.25	87	102.13	1.17		
9	26.19	0	620	24.44	.0394	2.00	.125
11	33.19	31.19	488	36.25	.0742		
12	33.19	67.69	353	66.25	.188		
13	33.19	97.69	217	96.62	.445		
14	27.19	128.19	71	102.62	1.45		
15	29.19	128.19	120	100.62	.837		
16	26.19	128.19	46	103.62	2.25		
17				NO LOAD			
18				NO LOAD		1.50	.167
19	15.19	0	351	13.44	0.0383		
21	17.69	37.69	243	21.75	.0896		
22	18.69	57.69	178	40.75	.229		
24	19.69	96.69	27	78.75	2.92		
25	19.69	91.69	50	73.75	1.48		
26	19.69	86.89	72	68.75	.957		
27	7.19	0	156	5.44	.0349	1.00	.250
29	9.19	18.19	123	10.75	.0874		
30	10.19	30.37	93	21.93	.236		
31	11.19	44.69	53	35.25	.665		
33	11.19	52.69	18	43.25	2.41		
34	11.19	48.69	36	39.25	1.09		
35				NO LOAD			
36	4.69	0	95	2.94	.0310	.750	.333
38	6.69	13.31	84	8.37	.0997		
39	6.69	20.19	53	15.25	.288		
40	6.69	27.19	22	22.25	1.01		
41	6.69	31.95	1.2	27.00	2.35		
42	6.69	29.19	13	24.25	1.87		
44				NO LOAD			

Where $V = P_1 - P_2 - 1.75$

$M_o = 24.46\ P_1 - 4.48\ P_2 - 19.8$

APPENDIX D

SAMPLE CALCULATIONS

1. **Photoelastic Analysis:**

Fringe order corresponding to σ_o = $\dfrac{\sigma_o}{\text{Fringe Constant}}$ = $(F.O.)_b$

$\dfrac{\sigma_f}{\sigma_o}$ = $\dfrac{\text{Corrected observed fringe order}}{(F.O.)_b}$

Run	Station	Fringe Order	Fringe Upper	Order Lower	Positions Average	Corr. F.O.	$(F.O.)_b$	$\frac{\sigma_f}{\sigma_o}$
38	.044	-1.0				-1.0*	4.1	-.24
	.100	-1.0				-1.0	4.1	-.24
	.170	2.0				2.0	4.1	.73
	.204	3.0				3.0	4.1	.49
	.235	4.0				4.0	4.1	.98
	.286	5.0				5.0	4.1	1.22
	.500	5.0	.38	-				
		6.0	.49	.40				
		7.0	.59	.51				
		8.0	.68	.63	See Figure XXXIV-C			
		9.0	.77	.73				
		10.0	.86	.84				
		11.0	.95	.95		5.1	4.1	1.24
	.694	5.0				5.0	4.1	1.22
	.767	4.0				4.0	4.1	.98
	.803	3.0				3.0	4.1	.73
	.835	2.0				2.0	4.1	.49
	.915	1.0	.41	.41	.41			
		1.0	.51	.41	.46			
		2.0	.65	.57	.61			
		3.0	.79	.69	.74			
		4.0	.93	.85	.89	See Figure XXXIV-C		
		5.0	1.11	1.01	1.06			
		6.0	1.29	1.17	1.23			
		7.0	1.47	1.35	1.41			
		8.0	1.65	1.53	1.58	-1.2	4.1	- .29

2. **Heller's Analysis:**

Modification of Equation 31b of Appendix A-I for an ovaloid of aspect ratio of 2.0 gives:

$$\frac{\sigma_f}{\sigma_c} = \frac{4.508 \sin\beta + 13.51 \frac{c}{b} \frac{\tau}{\sigma} \sin 2\beta - 2.592 \sin 3\beta - .193 \sin 5\beta}{2.800 - 1.743 \cos 2\beta + .752 \cos 4\beta}$$

*A negative sign indicates a stress opposite in sign to that expected for bending in the web without the hole.

For runs 1, 9, 19, 27, and 36 the origin of β is as indicated in Appendix A-I. For all other runs the origin is as indicated below:

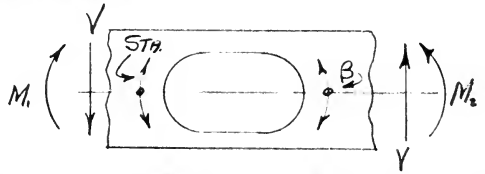

Run	Station	β	M (in-lbs)	V (lbs)	$\frac{\tau}{\sigma} = .125\ \frac{V}{M}$	$\frac{\sigma_+}{\sigma_o}$
36	0.0	0		2.94		0.0
	.131	30	95		.00387	-.192
	.175	40	95		.00387	.488
	.282	60	95		.00387	1.28
	.500	90	95		.00387	1.30
	.718	120	95		.00387	1.19
	.825	140	95		.00387	.371
	.869	150	95		.00387	-.571
	1.00	180		↓		0.0

3. Secondary Bending Analysis

Run	Station	M (in-lbs)	$\frac{y}{I}t$	σt	V' (lbs)	$\frac{y'l}{I'}$	$\frac{V'y'l}{I'}t$	σ_+	$\frac{\sigma_+}{\sigma_o}$
36	0.0	95	—	—	2.94	—	—	—	0.0
	.164	95	2.01	277		17.0	50.0	327	.970
	.240	95	3.35	318		15.2	44.7	363	1.08
	.306	95	3.55	337		12.0	35.3	372	1.10
	.500	95	—	—		—	—	—	1.00
	.694	95	3.55	337		12.0	-35.3	302	.896
	.760	95	3.35	318		15.2	-44.7	273	.810
	.836	95	2.91	277		17.0	-50.0	227	.673
	1.00	95	—	—	↓	—	—	—	0.0

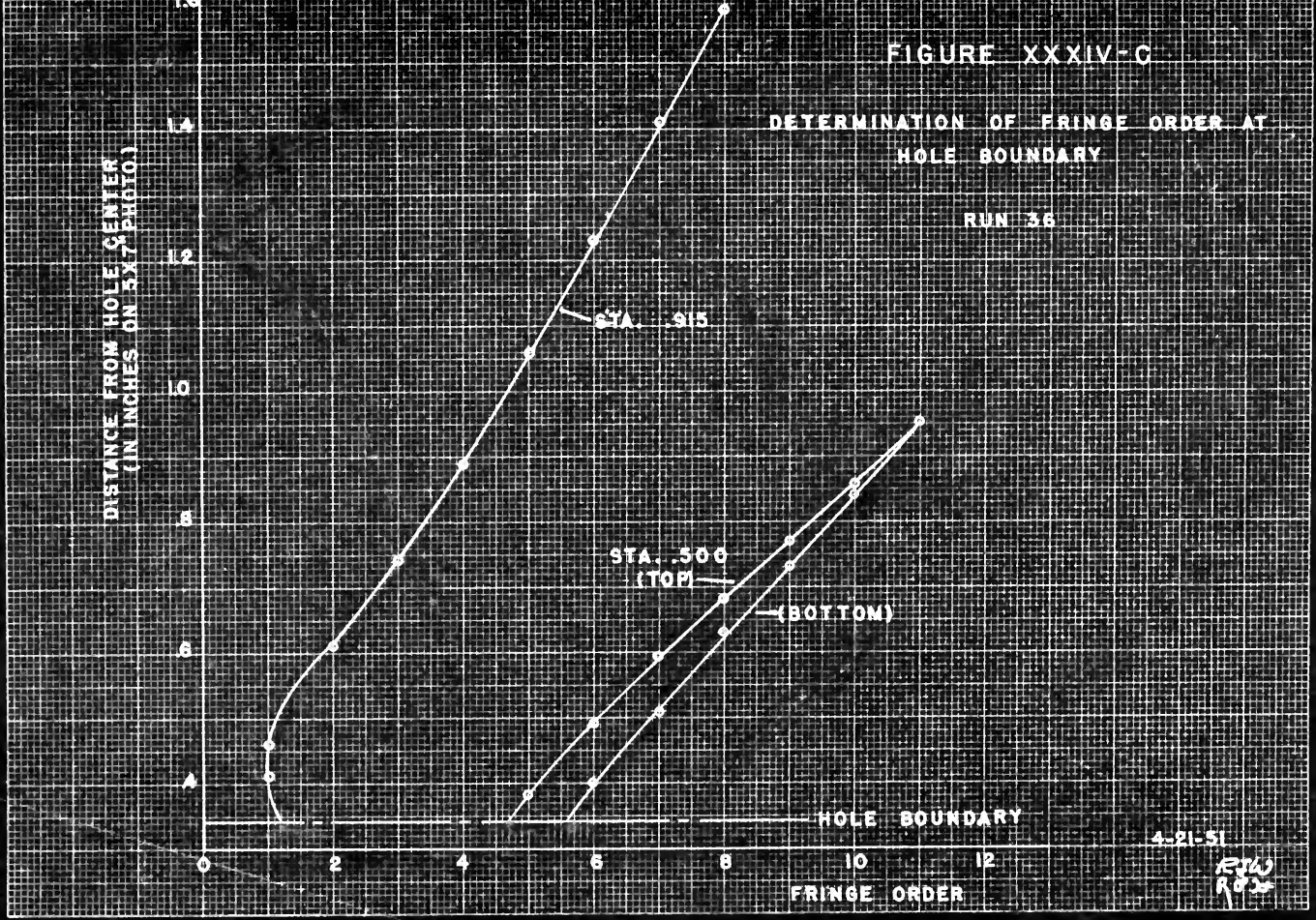
FIGURE XXXIV-C
DETERMINATION OF FRINGE ORDER AT HOLE BOUNDARY
RUN 36
DISTANCE FROM HOLE CENTER (IN INCHES ON 5"x7" PHOTO.)
STA. .915
STA. .500 (TOP)
(BOTTOM)
HOLE BOUNDARY
FRINGE ORDER
0
2
4
6
8
10
12
14
4
6
8
10
12
4-21-51
RTW
ROS

APPENDIX E

ORIGINAL DATA

The original data is presented in the form of the photographs of model isochromatics for all runs. (Figures XXXV-XXXIX.) Refer to Table II, Appendix C, for loadings.

FIGURE XXXV

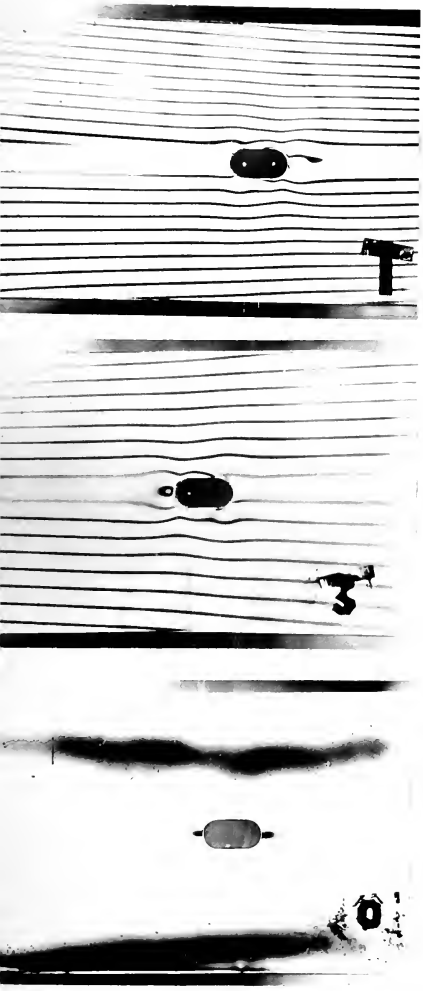

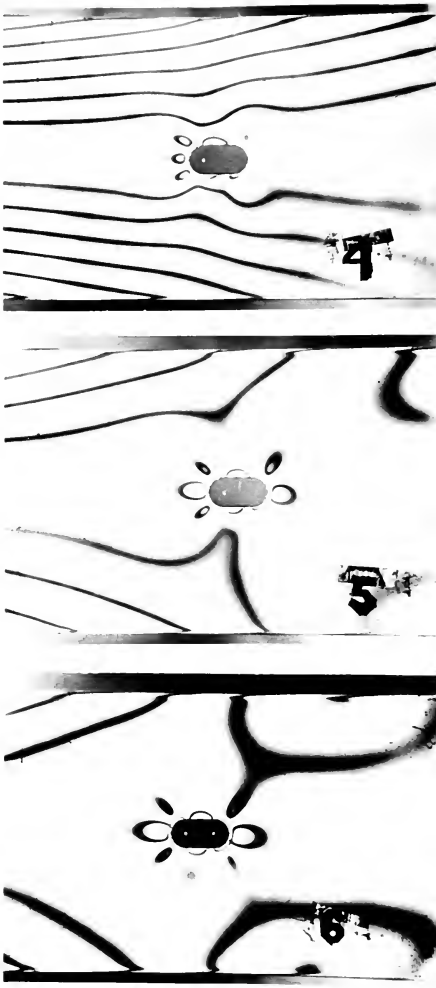

RUNS 0 - 6

$\frac{b}{c}$ = .100

FIGURE XXXVI

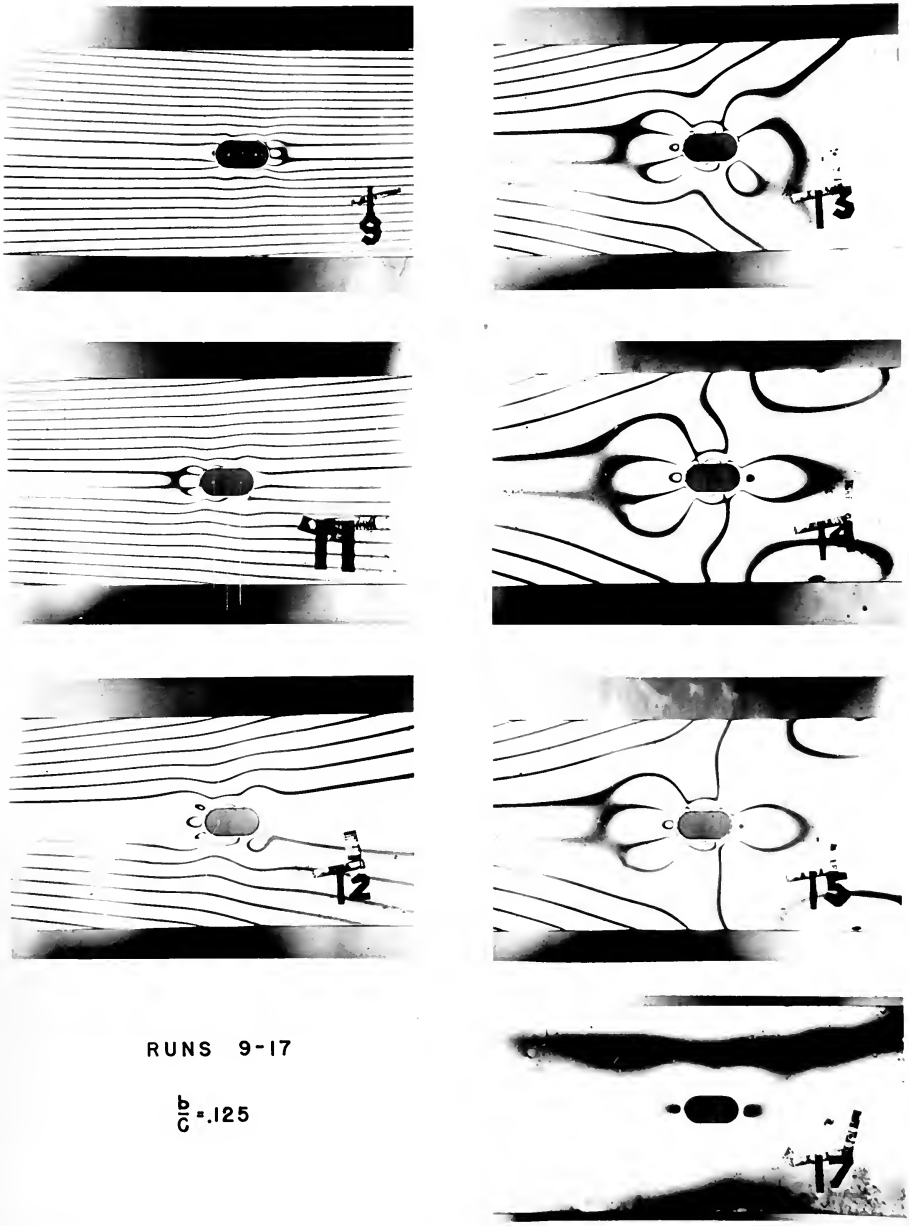

RUNS 9-17

$\frac{b}{c} = .125$

FIGURE XXXVII

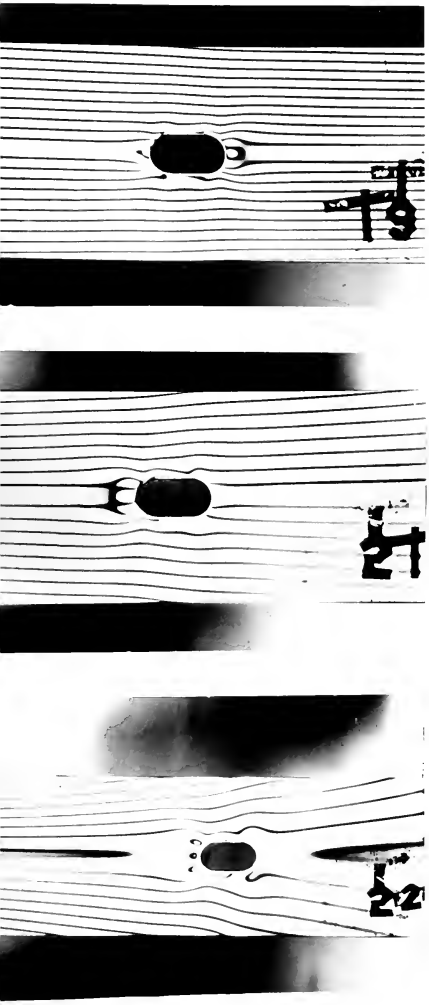

RUNS 18-26

$\frac{b}{C}$ = .167

FIGURE XXXVIII

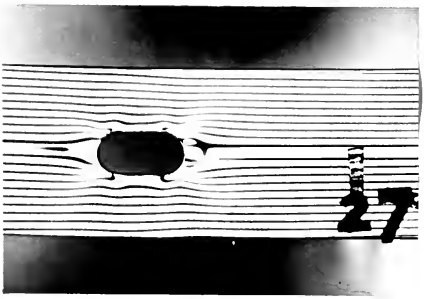

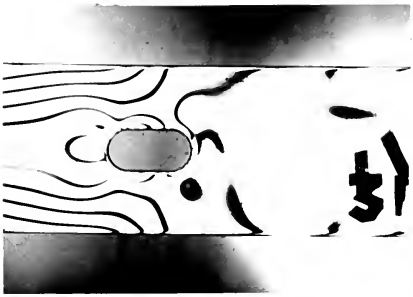

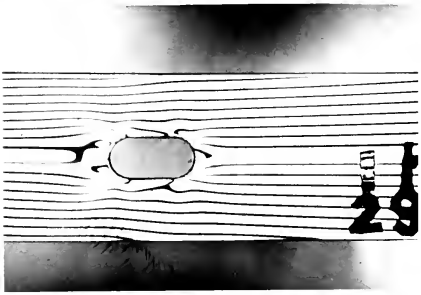

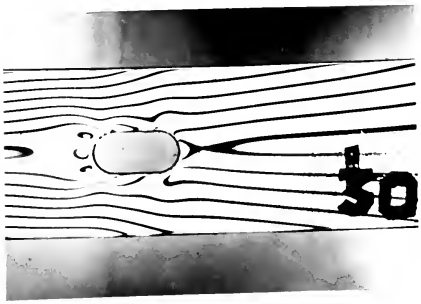

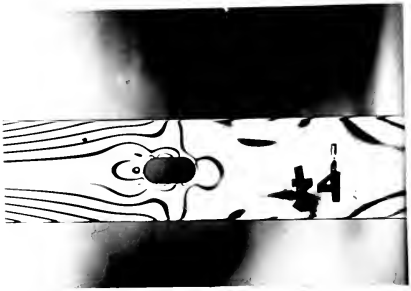

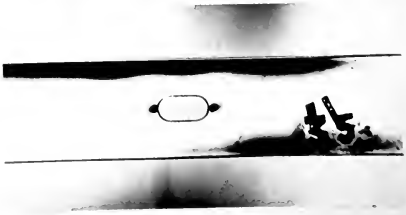

RUNS 27-35

$\frac{b}{c} = .250$

FIGURE XXXIX

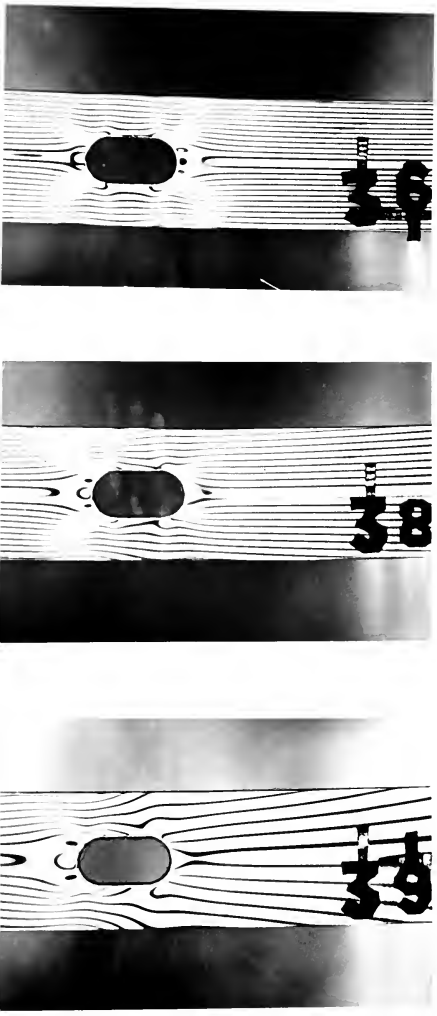

RUNS 36-44

$\frac{b}{C} = .333$

APPENDIX F

BIBLIOGRAPHY

(1) Greenspan, M.; Effect of a Small Hole on the Stresses in a Uniformly Loaded Plate, Quarterly Applied Mathematics, Vol.2, 1944, pp.60-71.

(2) Frocht, M.M.; "Photoelasticity," John Wiley and Sons, Inc., 1944.

(3) Howland, R.J.C., and Stevenson, A.C.; "Biharmonic Analysis in a Perforated Strip," Philosophic Transactions of the Royal Society of London, Series A, Vol. 232, 1933, pp.155-222.

(4) Inglis, C.E.; "Stresses in a Plate Due to the Presence of Cracks and Sharp Corners," Transactions of the Institution of Naval Architects, Vol. 55, London, 1913, pp.219-242.

(5) Joseph, J.A. and Brock, J.S.; "The Stresses Around a Small Opening in a Beam Subjected to Pure Bending," Paper 50-APM-3, American Society of Mechanical Engineers, 1950.

(6) Karl, L.R., Heller, S.R., and Gerich, W.R.; "The Effect of Small Holes on the Stress Distribution in Webs Subjected to Pure Bending," Graduate Thesis, Course XIII-A, M.I.T.

(7) Kirsch, G.; "Die Theorie Der Elastizitatuud Die Bedurfnisse Der Festigkeitslehre," Zeitschrift Des Versines Deutschner Ingenieure, Vol.42, 1898.

(8) Markovin, V., "Effect of a Small Hole on the Stresses in a Uniformly Loaded Plate," Quarterly of Applied Mathematics, Vol.2, No.4, 1944.

(9) Montgomery, J.B.; "An Investigation of Stress Due to Secondary Bending in a Structural Member",M.I.T.Thesis,1948.

(10) Neuber, H.; "Theory of Notch Stresses" David Taylor Model Basin, Translation No. 74, Nov. 1945.

(11) Tuzi, Z.; "Effect of a Circular Hole on the Stress Distribution of a Beam Under Uniform Bending Moment," Scientific Papers of the Tokyo Institute of Physical and Chemical Research, Vol.9, Aug.20, 1928, pp.65-89.

BIBLIOGRAPHY -- continued

(12) Wolf, K.; "Beitrage zur ebenen Alastizitatstheorie," Zeitschrift fur Technische Physik, Vol.2, No.8, 1921, p.209, and Vol.3, No.5, 1922, pp.160-166.

(13) Durelli, A.J.,and Murray, W.M.; "Stress Distribution Around a Circular Discontinuity in any Two-Dimensional System of Combined Stress," Proceedings of the Fourteenth Semi-Annual Eastern Photoelasticity Conference, New Haven Printing Co., Dec. 1941.

(14) Durelli, A.J.,and Murray, W.M.; "Stress Distribution Around an Elliptical Discontinuity in any Two-Dimensional, Uniform and Axial System of Combined Stresses," Experimental Stress Analysis, Vol.I, No.1, Addison-Wesley Press,Inc., Cambridge, Mass., 1943.